OPEN ACCESS

University of Dundee

University of Dundee

Effect of currents on nonlinear waves in shallow water

Kumar, Arun; Hayatdavoodi, Masoud

Published in:
Coastal Engineering

DOI:
10.1016/j.coastaleng.2023.104278

Publication date:
2023

Licence:
CC BY

Document Version
Publisher's PDF, also known as Version of record

Link to publication in Discovery Research Portal

Citation for published version (APA):
Kumar, A., & Hayatdavoodi, M. (2023). Effect of currents on nonlinear waves in shallow water. *Coastal Engineering*, *181*, [104278]. https://doi.org/10.1016/j.coastaleng.2023.104278

General rights
Copyright and moral rights for the publications made accessible in Discovery Research Portal are retained by the authors and/or other copyright owners and it is a condition of accessing publications that users recognise and abide by the legal requirements associated with these rights.

• Users may download and print one copy of any publication from Discovery Research Portal for the purpose of private study or research.
• You may not further distribute the material or use it for any profit-making activity or commercial gain.
• You may freely distribute the URL identifying the publication in the public portal.

Take down policy
If you believe that this document breaches copyright please contact us providing details, and we will remove access to the work immediately and investigate your claim.

Download date: 03. Sep. 2023

Coastal Engineering 181 (2023) 104278

Contents lists available at ScienceDirect

Coastal Engineering

journal homepage: www.elsevier.com/locate/coastaleng

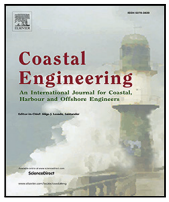

Effect of currents on nonlinear waves in shallow water

Arun Kumar [a], Masoud Hayatdavoodi [a,b,*]

[a] Civil Engineering Department, School of Science and Engineering, University of Dundee, Dundee DD1 4HN, UK
[b] College of Shipbuilding Engineering, Harbin Engineering University, Harbin, China

ARTICLE INFO

Keywords:
Wave–current interaction
Uniform current
Shear current
Cnoidal waves
Opposing current
Following current

ABSTRACT

Effect of various forms of currents on regular nonlinear waves in shallow water is investigated by use of a computational fluid dynamics approach. A range of wave conditions with different wave heights and wave periods are considered. Effect of three types of currents on these waves is investigated, namely (i) uniform current over the water depth, (ii) shear current from the seafloor to the still-water level, and (iii) a custom current profile that changes over the water depth. The current profiles are considered in both following and opposing directions of the incoming wave, forming in total 18 wave–current configurations. The Navier–Stokes equations for a laminar flow are solved computationally in two dimensions. A numerical wave–current maker is created to generate combined nonlinear waves and currents in shallow water. The effect of the currents on the change of the wave field, including quantitative change of the surface elevation, wave height, wavelength, horizontal particle velocity, and the velocity and pressure fields is presented and discussed. It is found that presence of the current can alter the wave field significantly, and the current profile and direction play a significant role in the change of the wave field. A following current in shallow water increases the peak of surface elevation, horizontal particle velocity and pressure, along with an increase in wavelength and wave height, while an opposing current reduces these. The change of wave height with current direction appears to be opposite to that observed in deep water in the literature. It is also concluded that a linear superposition of the undisturbed wave and current velocities can describe the horizontal particle velocity of the wave–current field for following currents (particularly under the wave trough) reasonably well, but larger differences are observed for opposing currents.

1. Introduction

The interaction between ocean waves and currents changes the wave properties, particularly in shallow water where currents can be stronger (Jeans et al., 2003; Carollo et al., 2005; Shen et al., 2008; Sheikh and Brown, 2010; Jeans et al., 2012). Soulsby et al. (1993) have pointed out that the combined effect of waves and currents in coastal zones influences the movement of sediment on the sea-bed, and the consequent evolution of the coastal morphology. It is also observed that the interaction between waves and currents affects the wave refraction and diffraction by an uneven seafloor (Liau et al., 2011). Tao and Han (2002) observed that pollutants move differently in the presence of combined waves and currents, when compared to waves-only condition, and this is partially due to the transformation of the wave field due to the ambient current.

According to Toffoli et al. (2013), stable wave packets can become unstable and break due to the presence of an opposing current (i.e., wave and current propagating in the opposite direction). The ability to predict the behaviour of waves as they interact with currents provides further information for mitigating the impact of severe waves on coastal structures. As per Markus et al. (2013), the presence of currents influences the wave–structure interaction by introducing significant drag forces, that along with the wave-induced loads, change the total load generated by the wave field. This implies that the presence of currents changes the wave-induced load.

It is important to understand the effect of currents on the coastal wave field in particular, where current modifies the wave transformation and their impact on structures. In shallow water, the water particle velocities are extended throughout the water depth, while these are negligible further away from the free surface in deep waters. Consequently, particle velocities and hence the wave field, can be affected more significantly by current in shallow water. Therefore, it stands to reason that the change in wave parameters would be different in shallow water when compared with deep water. It is understood that the wave properties, under the influence of a current, cannot be presented as a linear superposition of the wave properties and the current

* Corresponding author at: Civil Engineering Department, School of Science and Engineering, University of Dundee, Dundee DD1 4HN, UK.
E-mail address: mhayatdavoodi@dundee.ac.uk (M. Hayatdavoodi).

https://doi.org/10.1016/j.coastaleng.2023.104278
Received 26 September 2022; Received in revised form 29 December 2022; Accepted 7 January 2023
Available online 10 January 2023
0378-3839/© 2023 The Authors. Published by Elsevier B.V. This is an open access article under the CC BY license (http://creativecommons.org/licenses/by/4.0/).

properties (Kemp and Simons, 1982; Umeyama, 2011), hence, a detailed investigation of the nonlinear wave–current interaction process is required.

Several experimental studies have investigated the interaction between waves and currents in deep and finite water depths. Most have considered currents that (i) maintain a uniform profile across the water depth or (ii) change non-uniformly across the water depth, varying as a linear or quadratic function. The interaction of waves with following (current moving in the same direction as the waves) and opposing currents propagating over a rippled bed was studied experimentally by Brevik and Aas (1979) and by Brevik (1980) for a smooth bed. They observed that in case of following current, wavelength, λ, increases and wave height, H, decreases, whereas, in case of opposing current, wave height increases and wavelength decreases. These, however, were confined to deep water waves and were hindered by the degree of turbulence in the current. The interaction between linear waves and various non-uniform opposing currents was studied experimentally and numerically by Thomas (1981). It was observed that as the wave interacts with opposing currents of increasing velocities, the wavelength becomes smaller and wave height becomes larger. The waves were confined to deep water conditions, and only one current profile was investigated.

An experimental study of the interaction between gravity waves and currents with a uniform profile was conducted by Kemp and Simons (1982) in a laboratory channel with rough and smooth beds. The bed shear stress, mean velocity profile and wave attenuation were measured for waves with varying wave heights (with a fixed wave period, T) as they interacted with a non-uniform current. It was found that the mean velocity profile proposed by a linear superposition of wave and current velocities was remarkably different from those observed experimentally. The study considered different deep water wave conditions but the current profile remained unchanged. The waves considered were within the near-linear regime and wave effects higher than second order were not considered. An experimental and numerical study of nonlinear waves interacting with non-uniform currents was conducted by Thomas (1990). The wave height was found to be increasing and the wavelength was found to be decreasing, when the velocity of the current opposing the wave direction increased. The investigations of Thomas (1981, 1990) demonstrate that the interaction of linear and nonlinear waves with currents of increasing velocities results in similar trends in the change in wave height and wavelength in deep water conditions. These studies were limited to only one current profile. Effect of shearing current near the free surface was not investigated.

The change in wave period of a deep water wave due to a uniform current, also known as the Doppler-shifted period, was studied experimentally by Swan (1990) for a nonlinear wave interacting with a uniform current. The results were compared with the theoretical Doppler-shifted solution (Fenton, 1985). It was observed that the horizontal particle velocity, u_x, and surface elevation, η, in case of uniform currents were accurately predicted by the use of Doppler-shift method, whereas, depth-dependant currents required an alternate approach. The consequences of wave–current interaction were investigated by Lodahl et al. (1998) using an oscillatory flow coexisting with a current in a pipe. The current velocity was found to be a governing factor in determining the transition to turbulence in case of combined wave–current interaction.

Swan et al. (2001) studied experimentally the interaction of two-dimensional surface water waves with depth-varying currents. A uniform current was considered in the study along with a following and opposing mixed profile current that maintains a uniform profile up to a certain depth and then evolves linearly with water depth thereafter. The changes in wavelength and wave height, due to the presence of following and opposing currents, were assessed for different wave periods. It was observed that in case of following current interaction, the wave height becomes smaller, while in case of an opposing current interaction, the wave height becomes larger. The study was confined to only uniform current profile. The focus of the study is mostly on outlining the significance of vorticity distribution in case of wave interaction with a strongly sheared current.

Umeyama (2005) studied experimentally the effect of current direction on the mean velocity distribution by investigating the interaction of a nonlinear deep water wave with following and opposing uniform currents. The results were then compared with the theoretical data obtained using phase-averaged Prandtl momentum transfer theory and third-order Stokes wave theory. Assessment of the mean velocity profile showed that in case of waves interacting with a following current, a higher velocity was observed close to the tank floor and a lower velocity was observed above a certain water depth, relative to the logarithmic profile. The opposite was observed as the wave interacted with an opposing current.

Umeyama (2009) conducted an experimental study of the interaction between waves and following and opposing uniform currents. The changes in Reynolds stress, velocity distributions and turbulent intensity due to the wave–current interaction, were assessed by obtaining the vertical, lateral and horizontal velocity components. The study expands the work done by Umeyama (2005), which did not assess the phase-averaged velocity and lateral turbulence. In case of a following current, the mean horizontal velocity was observed to increase further away from the seabed until half the water depth and then decrease gradually. An experimental study of the interaction between waves and uniform current focusing on particle velocities and trajectories was conducted by Umeyama (2011). It was found that in case of following current, the wave height of a wave-only condition was 13%–17% larger than a wave–current interaction condition. Umeyama (2011) pointed out that a linear superposition of the water particle velocity due to waves and the current velocity does not correctly predict the horizontal particle velocity distribution.

Ruggeri and Faraci (2022) experimentally studied the generation and evolution of ripples and the dynamics of the vortex structure generated under combined wave–current setup. They observed that bedforms take longer to stabilize when the current is superimposed onto the wave. While the present study only considers a flat seafloor, several investigations have been carried out assessing the wave–current interaction over rough beds, see e.g., Fredsøe et al. (1999), Petrotta et al. (2018) and Hsiao et al. (2020).

Several numerical studies have been carried out to assess the interaction of waves and currents. Dalrymple (1974) carried out a theoretical assessment of the wave–current interaction between waves and a following current by modifying the Stream Function wave theory to include a bi-linear shear current. It was found that as waves interact with different currents, the wavelength and the maximum horizontal particle velocity exhibit large disparities. Their theoretical approach, however, assumed that the waves were long-crested and propagated without change in form. The interactions of currents and weakly nonlinear water waves in shallow water were studied using Boussinesq-type depth-averaged equations derived by Yoon and Liu (1989). The current velocity was assumed larger than the characteristic wave orbital velocity, but smaller than the wave group velocity. Only a uniform current was chosen aiming to develop a set of equations that could be used to study the interactions between waves and currents in shallow water.

The study conducted by Chen et al. (1999) focused on the effects of uniform currents on near-resonant triad interactions of gravity waves in shallow water. Boussinesq-type equations for the fully coupled wave–current interaction were utilized to set up the numerical wave tank. They found that an opposing current increased the magnitude of phase mismatch (phase difference between wave–current and wave-only cases), while the opposite was observed for a following current. It was also observed that an opposing current increased the wave height, reduced the Ursell number, beat-length, and the ratio of the energy in higher harmonics to the energy in the primary wave in comparison with the pure wave motion in shallow water. On the other hand, a

following current intensified the extent of triad interactions. Chen et al. (1999) noted that this was in contrast to the current influence on quadruplet interactions of deep water waves. The study was confined to one current profile in shallow water conditions.

By deriving an asymptotic model for long surface gravity waves of large amplitude in shallow water, the interaction between a linear shear current and a strongly nonlinear solitary waves was investigated by Choi (2003). The study used the Korteweg–de Vries (KdV) equation for solitary waves. It was observed that while interacting with a following current, a solitary wave narrows down, whereas when the current opposes the direction of wave propagation, it widens.

Based on the analytical solutions of periodic waves propagating over a uniform current, the interaction between nonlinear water waves and a uniform current was studied by Hsu et al. (2009). The variations in the water particle orbits and the wave profile resulting from the interaction with a steady uniform current of varying velocities were studied. It was observed that the relative horizontal distance travelled by a water particle was larger in case of following current interaction, whereas the opposite was observed in the case of an opposing current.

Zhang et al. (2014) investigated the interaction between following and opposing uniform currents and a solitary wave using a numerical model based on the Reynolds-Averaged Navier–Stokes (RANS) equations. It was observed that an increase in current velocity led to an increase in the effective wavelength. It was also observed that the wave height of a solitary wave decreased as it interacted with following currents while the opposite was observed in case of opposing currents. The interaction of nonlinear water waves and a linear shear current was studied by Guyenne (2017) using a two-dimensional direct numerical simulation method for solving the time-dependent equations based on Stokes wave theory. The theory describes the nonlinear water waves over uniform depth with a non-zero constant vorticity. It was observed that following currents stabilized the surface wave dynamics. In addition to Stokes waves in deep waters, the study also considers solitary waves, but was confined to only one current profile.

Duan et al. (2018) studied the steady solution of a solitary wave propagating in the presence of a linear shear background current using the high-level Green–Naghdi (HLGN) equations. It was found that the results agree well with the observations of Choi (2003). Wang et al. (2020) investigated the steady solutions of solitary waves in the presence of non-uniform shear currents using the HLGN equations. It was shown that the velocity field and the vorticity field of the solitary wave were modified due to the presence of non-uniform shear current. Formation of a vortex under the wave crest was observed in the presence of opposing shear currents. The vertical position of the vortex increased under the linear, quadratic and cubic current profiles, respectively.

Chen and Zou (2019) studied numerically, the effect of vertically sheared following and opposing current profiles, on a nonlinear wave by solving the Navier–Stokes (NS) equations computationally. It was observed that in the presence of following vertically sheared current, the wave exhibited a sharper crest and flatter trough, while the opposite was observed in the presence of an opposing vertically sheared current. The study investigated the near resonant triad interactions in shallow water and considered currents with different profiles.

From the assessment of the experimental and numerical studies conducted on wave–current interaction, it is observed that the effect of various current profiles on nonlinear shallow water waves and of varying properties has remained unexplored. The behaviour of currents observed from oceanographic data (see e.g., Jeans et al. (2003), Carollo et al. (2005), Shen et al. (2008), Sheikh and Brown (2010) and Jeans et al. (2012)) suggests that the current profile changes with geographic locations and time. This is especially significant in shallow water, where the particle velocity would be strongly influenced by currents throughout the water depth. Hence, the wave–current loading on coastal structures would be affected by the nature of the current profile interacting with the wave. Therefore, it is imperative to assess the effect of different current profiles on shallow water waves.

Our goal in this study is to assess the change in the behaviour of nonlinear waves in shallow water, as they interact with currents with different profiles and directions. Specifically, the effect of these currents on the surface elevation, wave height, wavelength, horizontal particle velocity, velocity profile and pressure is investigated. While only two-dimensional following and opposing current directions are considered in the present study, several investigations have been carried out in three-dimensions assessing the orthogonal wave–current interaction in coastal waters (i.e., wave and current approaching each other at angles other than 0° or 180°), see e.g., Lim and Madsen (2016) and Faraci et al. (2018, 2021).

The theory pertaining to the computational method used in this study and the computational approach taken to solve the governing equations are discussed in Section 2. The setup of the numerical wave–current tank is presented in Section 3. Discussion leading to the selection of various waves and current profiles considered in this study is presented in Section 4. Finally, comparison of the results of the numerical wave tank with experimental studies, the results of the wave–current study and their implications are discussed in Section 5, followed by concluding remarks.

2. Theory and numerical solution

A two-dimensional Cartesian coordinate system is used, where waves propagate in the positive $x-$direction (to the right), and z is the vertical axis, positive against the gravitational acceleration. The origin of the coordinate system is at the still water level (SWL). For the scale at which it is observed, the fluid is assumed to be a homogeneous, Newtonian, incompressible continuous substance. We assume that the consequences of turbulence are negligible in this problem of wave–current propagation over a flat seafloor, see e.g., Chen et al. (2014, 2019) and Chen and Zou (2019), for applications of laminar flow in solving the wave–current interaction problem. For studies on wave–current interaction using a turbulence model, see e.g., Zhang et al. (2014, 2015) and Bai et al. (2017). The fluid pressure and velocity are considered differentiable at all times and everywhere in the domain. The flow is governed by the mass and momentum conservation equations,

$$\vec{\nabla}.\vec{V} = 0, \tag{1}$$

$$\frac{\partial \vec{V}}{\partial t} + \nabla\vec{V}.\vec{V} = -\frac{1}{\rho}\nabla p + \nu\vec{\nabla}^2\vec{V} - \vec{g}, \tag{2}$$

where $\vec{V} = u_x\vec{i} + u_z\vec{k}$ is the velocity vector, with $\vec{i}$ and $\vec{k}$ being the unit normal vectors in $x-$ and $z-$ directions, respectively, p is the pressure, ν is the kinematic viscosity, ρ is the density of the fluid, t is time and $\vec{g}$ represents the body force vector due to gravity. The gradient function is represented by ∇. The divergence and laplacian vectors are represented by $\vec{\nabla}$ and $\vec{\nabla}^2$, respectively. Eqs. (1) and (2) are only solved in the $x-$ and $z-$ directions in this two-dimensional study. They are solved for both air on top and water phases simultaneously.

The pressure-velocity coupling problem is solved iteratively using the PIMPLE algorithm (Ferziger et al., 2002). Finite volume approach is used to discretize the governing equations. An open source computational fluid dynamics package, OpenFOAM, is used to carry out the computations. The Volume of Fluid method is used to capture the free surface between water and air (Hirt and Nichols, 1981).

The shallow water waves in this study are generated using the Cnoidal wave theory. Starting from the KdV equation, the surface elevation, particle velocity and pressure are obtained as

$$\eta = \eta_{min} + Hcn^2(\theta, m), \tag{3}$$

where, η_{min} is the distance between the SWL and the wave trough and cn is the Jacobian elliptic function of variables θ and m ($0 \leq m < 1$) (Svendsen and Jonsson, 1976). η_{min} is defined as

$$\eta_{min} = \left(\frac{1}{m}\left(1 - \frac{E}{K}\right) - 1\right) H, \tag{4}$$

where, $K = K(m)$ and $E = E(m)$ are the complete elliptical integrals of the first and second kind, respectively. The variable θ, in Eq. (3), is defined as

$$\theta = 2K\left(\frac{t}{T} - \frac{x}{\lambda}\right). \tag{5}$$

The horizontal particle velocity according to the Cnoidal wave theory is given as

$$u_w = c\left[\frac{\eta}{h} - \left(\frac{\eta}{h}\right)^2 + \frac{1}{2}\left(\frac{1}{3} - \left(\frac{z+h}{h}\right)^2\right) h\eta_{xx}\right], \tag{6}$$

where, c is the phase velocity, z is the vertical coordinate that varies from 0 to $-h$ and η_{xx} is obtained by differentiation of Eq. (3). Similarly, the pressure field under the Cnoidal wave is described by

$$p = \rho g\left[\eta + \frac{1}{2}h^2\left(1 - \left(\frac{z+h}{h}\right)^2\right)\eta_{xx}\right]. \tag{7}$$

Hereafter, acceleration due to gravity (g), density of water (ρ) and the water depth (h), are used as a dimensionally independent set to nondimensionalize all parameters. Therefore, $\overline{H} = H/h$, $\overline{\eta} = \eta/h$, $\overline{p} = p/\rho g h$, $\overline{T} = T/\sqrt{h/g}$, $\overline{u_x} = u_x/\sqrt{gh}$ and $\overline{\lambda} = \lambda/h$. The bar over the variables is removed from all dimensionless quantities for simplicity.

The combined wave–current field is generated by the use of a theoretical wave–current maker. The horizontal particle velocity at the wave–current maker is obtained by the linear superposition of the wave and the current velocities. Hence, the wave–current horizontal particle velocity (u_{wc}) for the combined current and wave, at the location of the wave-maker, is given by

$$u_{wc} = u_w + u_c, \tag{8}$$

where, u_w is the horizontal particle velocity due to the wave given in Eq. (6) and u_c is the horizontal particle velocity due to the current.

The numerical wave–current tank is made up of three sections: (i) the generation zone where the velocity, pressure field and free surface elevation are enforced, (ii) the computational region where the NS equations are solved iteratively, and (iii) the absorption zone where the wave–current system is allowed to gradually dissipate and die out, known as the wave–current absorption zone. The wave–current generation and absorption zones, also known as inlet and outlet relaxation zones, respectively, are modifications of those proposed by Jacobsen et al. (2012) for waves. The absorption zone is used to minimize the computational cost by restricting the length of the computational domain. The boundary condition of the wave–current absorption zone is modified from the default zero-velocity current to the current profile linearly superposed at the wave generation zone. The tank bottom is flat and stationary and the fluid velocity at this fixed boundary is set to 0, i.e. a no-slip boundary condition is imposed on this boundary. We have monitored the change in mass of the tank due to the different types of currents, and found that the maximum change in mass is 0.53%.

3. Numerical tank setup

In this section, the setup of the numerical wave–current tank and its computational mesh are introduced. In this study, a structured, hexahedral mesh is used for the spatial discretization of the numerical domain. The wavelength and wave height of the incident wave are used to define the refinement of the mesh. Different mesh configurations with increasing number of cells per wavelength and wave height are considered in the mesh convergence study as outlined in Table 1. The number of cells per wave height is varied between 40 and 80 and the number of cells per wavelength is varied between 250 and 750.

Table 1
Mesh configurations considered in the convergence study, $H = 0.2$, $T = 24.99$ and $h = 0.15$ m. Δx and Δz represent the size of the cell in $x-$ and $z-$directions, respectively.

Mesh	$H/\Delta z$	$\lambda/\Delta x$	Computational time
A	40	250	9 h 27 min
B	62	500	22 h 19 min
C	80	750	82 h 8 min

A shallow water wave with $H = 0.2$ and $T = 24.99$ ($h = 0.15$ m, fixed in all cases considered here, unless stated otherwise) is generated using different mesh configurations and the results are shown in Fig. 1. Here, time series of surface elevation recorded at distance λ from the inlet relaxation zone is compared with the analytical solution. Very small difference is observed between results of different mesh configurations. Mesh B, with 62 cells per wave height and 500 cells per wavelength is considered optimum and computationally reasonable for the cases of this study.

The two-gauge method outlined by Grue (1992) is employed to obtain the wave reflection at the centre of the domain. The reflection and transmission coefficients of strongly nonlinear waves were successfully computed by Hayatdavoodi et al. (2017) using this method. Two wave gauges are placed at the centre of the domain separated by distance 0.2λ, and the time series of surface elevation is obtained from these gauges. The incident and reflected wave amplitudes are separated using the Fourier transform of the time series. Finally, the reflection coefficient (C_R) is obtained as the ratio of the reflected wave amplitude to the incident wave amplitude. Fig. 2 shows the variation of C_R with time for a wave with $H = 0.2$ and $T = 24.99$. It is observed that the reflection from the outlet relaxation zone remains below 2% during these computations.

It is shown in Kumar and Hayatdavoodi (2023) that a numerical domain with an inlet relaxation zone of length λ and an outlet relaxation zone of length 0.75λ results in a stable and efficient domain for the wave–current field, with negligible reflection from the open boundary (less than 5% for the waves considered in this study). This is in agreement with the previous investigations of Hayatdavoodi et al. (2015) on the optimum computational domain length for nonlinear waves. Hence, the total length of the numerical wave tank is 7λ. This ensures that at least five waves are entirely outside the relaxation zones for the investigations while confining the computational cost. The schematic of the numerical wave tank is shown in Fig. 3. Surface elevation is recorded by Gauges GI, GII and GIII, placed at distances λ, 2λ and 3λ from the inlet relaxation zone, respectively. Pressure and velocity are recorded by sensors placed at distance λ from the inlet relaxation zone and at three different water depths, shown in Fig. 3.

4. Wave-current conditions

This study focuses on nonlinear waves propagating in shallow water in the presence of ambient currents. The waves and currents chosen in this study are discussed in this section. In the numerical wave–current tank, the water depth is fixed at 0.15 m in all cases (except for cases used in comparisons) and the wave parameters are altered to include seven nonlinear waves in shallow water depths, given in Table 2. For cases W1, W2, W3 and W5 the wave height is reduced successively, while keeping the wavelength constant, and for cases W6, W3, W4 and W7, the wavelength is increased successively, while keeping the wave height constant. These wave conditions are considered to investigate how the wave–current interaction changes with wave height and wavelength.

Three current profiles are considered in this study, namely uniform current profile, shear current profile and custom current profile. The horizontal particle velocity due to the current, u_c, evolves as a function of the water depth and is defined as

$$u_c(z) = U, \tag{9}$$

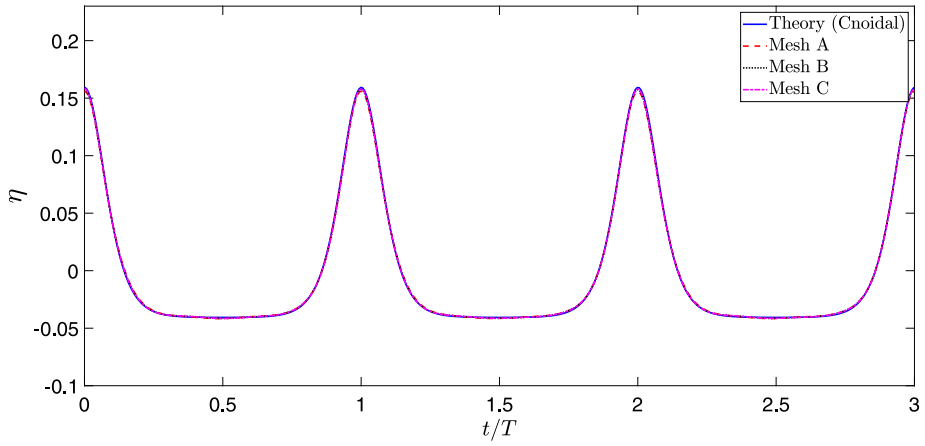

Fig. 1. Time series of surface elevation recorded at distance λ from the inlet relaxation zone for the three mesh configurations considered here, compared with the analytical solution in the absence of current, $H = 0.2$, $T = 24.99$ and $h = 0.15$ m.

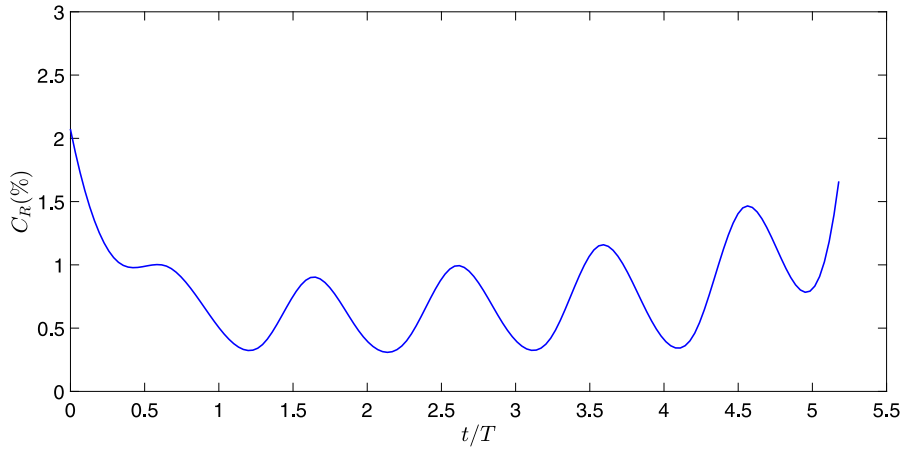

Fig. 2. Variation of wave reflection coefficient from the outlet relaxation zone of the numerical domain in the absence of current, $H = 0.2$ and $T = 24.99$.

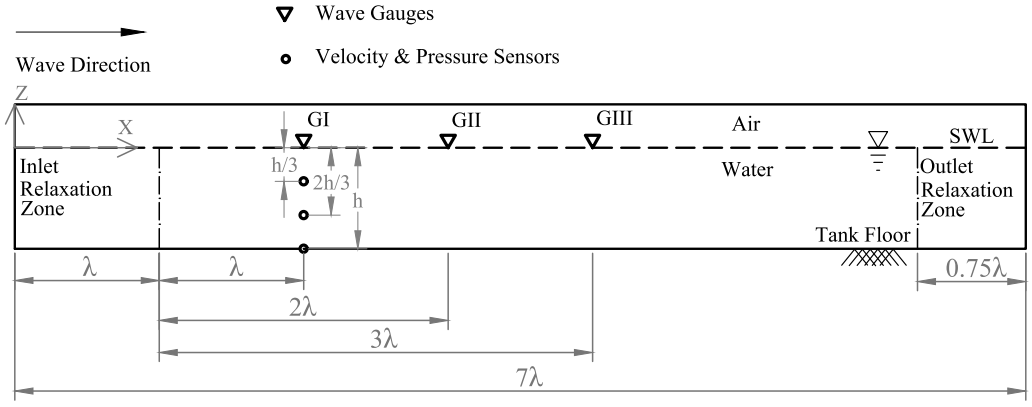

Fig. 3. Schematic of the numerical wave–current tank along with the location of the sensors. Figure not to scale.

for the uniform current,

$$u_c(z) = (z+1)\,U_f, \tag{10}$$

for the shear current, and

$$u_c(z) = \begin{cases} U & \text{for} \quad z < z_c \text{ and} \\ \left(\frac{U-U_f}{z_c}\right) z + U_f & \text{for} \quad z \geq z_c, \end{cases} \tag{11}$$

for the custom current profile, where, U_f is the current velocity at the free surface, U is the uniform current velocity and z_c is the vertical coordinate (measured from the SWL) at which the current profile changes from uniform to sheared. In this study, only $z_c = -0.5$ is considered. It is determined that a uniform current, a shear current and a custom current profile that maintains a uniform profile up to a certain water depth and a sheared profile thereafter, provide a reasonable representation of possible current profiles in shallow water. At $z_c \geq -0.5$, the profiles of custom and shear current are identical, while at $z_c \leq -0.5$, the custom and uniform current profiles are identical. These allow for a direct comparison of the effect of different current profiles. The selected current profiles are in agreement with the cases considered by Swan (1990), Swan et al. (2001), Umeyama (2005, 2011) and Son

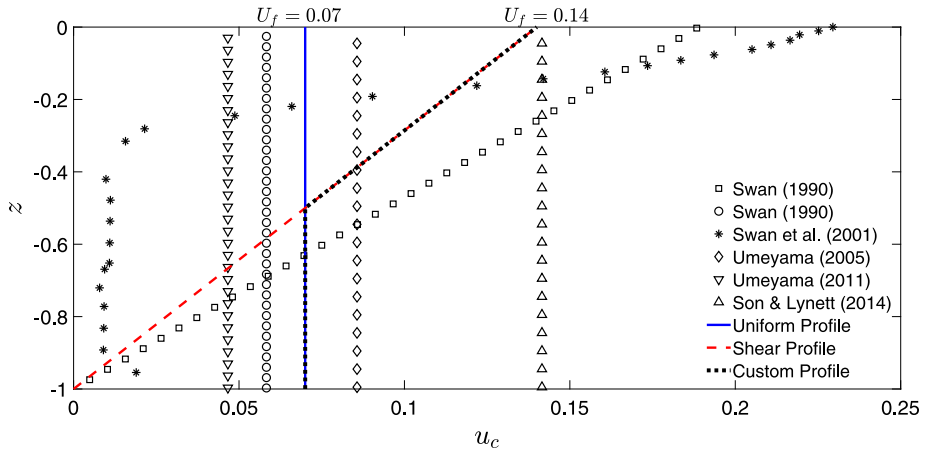

Fig. 4. Current profiles and velocities of this study (shown for the case of following current), along with other current profiles considered in the literature. In the case of opposing currents, the profiles are mirrored along the vertical axis with respect to $u_c = 0$.

Table 2
Wave conditions considered in this study (h = 0.15 m in all cases).

Case	Wave height H	Wavelength λ	Wave period T	Steepness (H/λ)	h/gT^2	H/gT^2
W1	0.4	26	23.45	0.015	0.001	0.0007
W2	0.3	26	24.18	0.012	0.0017	0.0005
W3	0.2	26	24.99	0.008	0.001	0.0003
W4	0.2	39	36.84	0.005	0.0007	0.00015
W5	0.1	26	25.80	0.004	0.001	0.0001
W6	0.2	13	13.22	0.015	0.005	0.001
W7	0.2	52	48.68	0.004	0.0004	0.00008

Table 3
Current types and velocities considered in this study.

Current type	Current velocity at the free surface (U_f)
Custom	±0.14
Shear	±0.14
Uniform	±0.07

and Lynett (2014). Table 3 provides details of the selected current profiles. Here, a positive current velocity indicates a following current and a negative current velocity indicates an opposing current.

Six current configurations are considered in this study by changing the current profile and direction relative to the wave propagation direction (following or opposing). These current configurations, along with the current data of some existing laboratory measurements are shown in Fig. 4.

First, a set of wave–current interaction cases are considered involving the wave condition W3 ($H = 0.2$ and $\lambda = 26$), for all six current configurations mentioned above. Then, the custom current profile with $U_f = \pm 0.14$ and $z_c = -0.5$ is considered for all seven wave conditions. These result in total 18 wave–current cases, listed in Table 4. The results of these wave–current interaction cases are then used to investigate the variation of surface elevation, wave height, wavelength, horizontal particle velocity, and the velocity and pressure fields with the current profile and direction, and for waves with different wave height and wavelength.

5. Results and discussions

The results obtained from the assessment of the numerical wave–current tank are discussed in this section. First, results of the NS model are compared with existing laboratory experiments and other computational studies. Then the wave conditions of this study and the wave–current interactions are studied. The investigations include changes in surface elevation, wave height, wavelength, horizontal particle velocity, velocity distribution and pressure distribution.

Table 4
Description of the 18 wave–current cases considered in this study. Both following (F) and opposing (O) current directions are investigated in all cases.

Case	Wave type	Current type
W1C1_F W1C1_O	W1	Custom
W2C1_F W2C1_O	W2	Custom
W3C1_F W3C1_O	W3	Custom
W3C2_F W3C2_O	W3	Shear
W3C3_F W3C3_O	W3	Uniform
W4C1_F W4C1_O	W4	Custom
W5C1_F W5C1_O	W5	Custom
W6C1_F W6C1_O	W6	Custom
W7C1_F W7C1_O	W7	Custom

5.1. Comparison with laboratory experiments

In this section, a coexisting wave–current field is generated using the numerical wave–current tank and results are compared with the laboratory measurements of Umeyama (2011) and results of the RANS model of Zhang et al. (2015). A wave with $H = 0.078$ and $T = 5.72$ propagates over a uniform current with $U = 0.0466$ in a tank with $h = 0.3$ m.

Time series of surface elevation of the wave–current field, recorded by a gauge located at distance 2λ from the inlet relaxation zone, is shown in Fig. 5. It is observed that results of the NS model generally agree with the computations of Zhang et al. (2015) and the laboratory measurements of Umeyama (2011). Fig. 6 shows the horizontal particle velocity distribution over the water depth under the wave crest and wave trough. It is observed that the horizontal particle velocity at the tank floor is zero, which complies with the no-slip boundary condition. As seen in Fig. 6(a), the horizontal particle velocity under the wave crest is larger than the uniform current velocity in the domain ($U = 0.0466$), whereas it is smaller than the uniform current velocity when observed under the wave trough in Fig. 6(b) and these are expected.

Next, the results of the NS model, for the wave–current cases considered here, are presented and discussed in the following five subsections, namely (i) change in surface elevation, (ii) change in wave

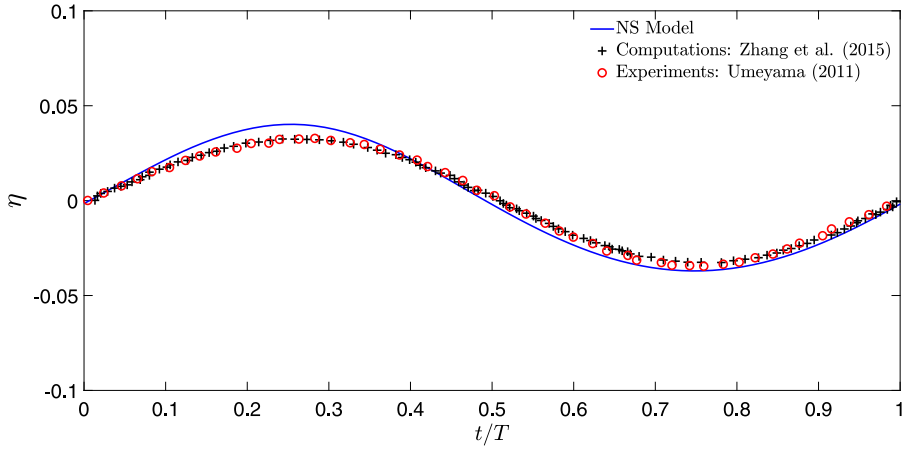

Fig. 5. Time series of the wave–current surface elevation, obtained by the NS model, and compared with laboratory measurements of Umeyama (2011) and computations of Zhang et al. (2015), $H = 0.078$, $T = 5.72$, $h = 0.3$ m and $U = 0.0466$.

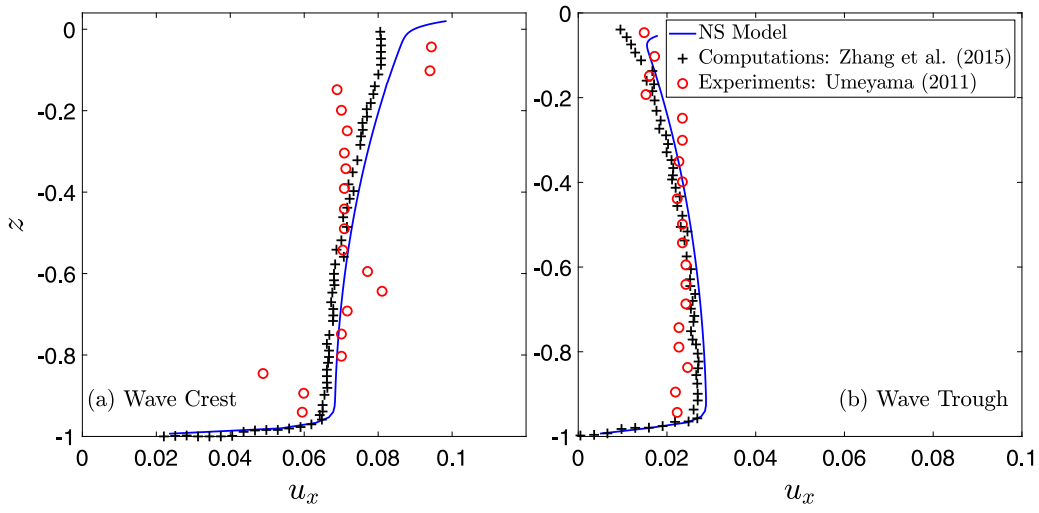

Fig. 6. Horizontal velocity distribution along the water column of the wave–current field, under the (a) wave crest and (b) wave trough obtained by the NS model, and compared with laboratory measurements of Umeyama (2011) and computations of Zhang et al. (2015), $H = 0.078$, $T = 5.72$, $h = 0.3$ m and $U = 0.0466$.

height and wavelength, (iii) change in horizontal particle velocity, (iv) change in velocity profile and (v) change in pressure. Each subsection is subdivided into two categories: (a) variable wave conditions, which is studied by observing the interaction of all seven waves with the custom current profile, and (b) variable current profiles, which is studied by observing the interaction of wave W3 with the six current configurations of this study.

5.2. Change in surface elevation

In this section, the surface elevation of the incident waves as they interact with different currents is investigated. Time series of the surface elevation recorded at Gauges GI, GII and GIII, in the absence of current, are shown in Fig. 7, along with the analytical solution for surface elevation obtained using the Cnoidal wave theory, Eq. (3). The waves generated in the tank are stable and in good agreement with the analytical solution. Next, currents are introduced into the domain and the surface elevation is studied, in the presence of current. The change in surface elevation is investigated by defining the change of the peak of surface elevation, $\eta' = [(\eta_{wc} - \eta_w)/\eta_w] \times 100$, where η_{wc} is the peak of wave surface elevation under the influence of the current and η_w is the peak of wave surface elevation in the absence of the current i.e. η' is the percentage change of the peak of surface elevation when compared with the wave-only cases. In order to obtain the peak of surface elevation at a given gauge, all waves excluding the ramp wave are observed, the maximum and minimum peak values are discarded and the mean of the remaining peaks in the signal is used for the analysis. This approach is also employed later while assessing the change of the horizontal particle velocity and the pressure.

5.2.1. Effect of the wave conditions

In this subsection, the change of surface elevation of all waves as they interact with the custom current ($U_f = \pm 0.14$ and $z_c = -0.5$) is studied (cases W1C1, W2C1, W3C1, W4C1, W5C1, W6C1 and W7C1 in Table 4). The surface elevation of the waves in the presence of the current, recorded at Gauge GI is shown in Fig. 8. It is observed that under the influence of current, the wave trough exhibits little to no change. Subsequently, only the change in wave crest is discussed quantitatively hereafter (i.e. the change of the wave amplitude). An enlarged view of the wave crest is also presented for all seven wave cases. The surface elevation of the incident wave is influenced by the current direction. In all seven waves, it is seen that a following current enlarges the wave crest whereas an opposing current results in smaller wave crests.

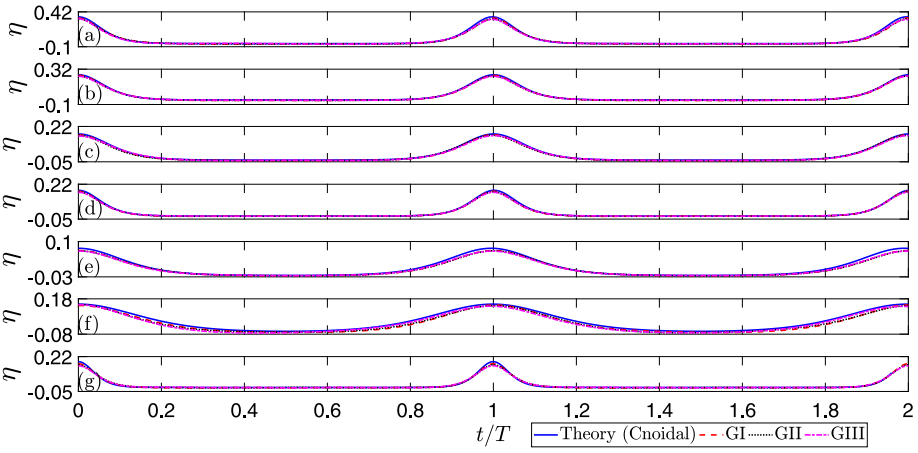

Fig. 7. Time series of surface elevation recorded at Gauges GI, GII & GIII for waves (a) W1, (b) W2, (c) W3, (d) W4, (e) W5, (f) W6 and (g) W7, in the absence of current.

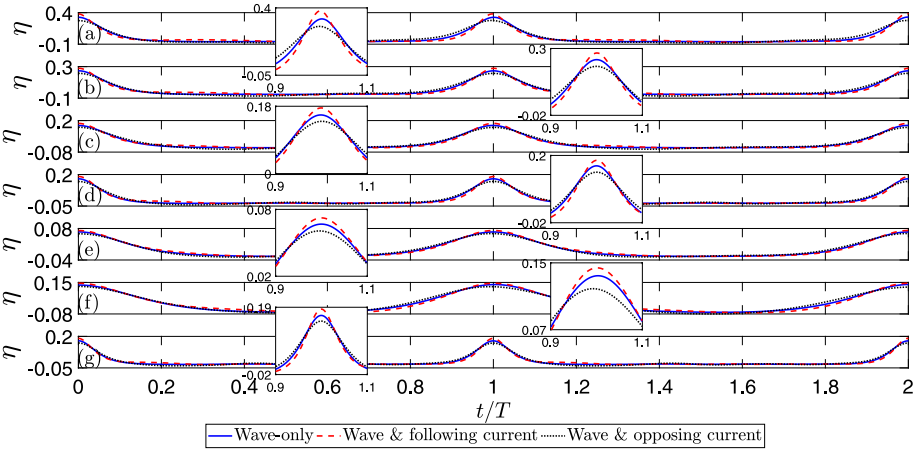

Fig. 8. Time series of surface elevation, recorded at Gauge GI, of waves (a) W1, (b) W2, (c) W3, (d) W4, (e) W5, (f) W6 and (g) W7, as they interact with following and opposing custom currents, $U_f = \pm 0.14$ and $z_c = -0.5$.

The change of the peak of surface elevation is shown in Fig. 9. From Fig. 9(a), it is inferred that the effect of the current on the peak of surface elevation of larger waves is more significant. As the wave height is increased successively, η' changes nonlinearly from 8% to 15%, for following currents, and from −9% to −19%, for opposing currents. Fig. 9(b) shows the change of the peak of surface elevation with wavelength, and it is observed that η' changes from 8% to 12%, for following currents, but remains invariant at about −10%, with increasing wavelength for opposing currents.

5.2.2. Effect of the current profiles

Interaction of wave W3 with the six current configurations chosen in this study is investigated in this subsection. The surface elevation data obtained from Gauge GI is used for this investigation. The interaction of wave W3 with following and opposing currents with shear, uniform and custom profiles is shown in Fig. 10; depicting the effect of changing current profile on surface elevation. A uniform current is observed to have a weaker impact on the surface elevation of the incident wave. Shear and custom current profiles result in almost identical change in the surface elevation. This indicates that the current profile near the free surface has the dominant effect on the surface elevation.

The corresponding change of the peak of surface elevation (η') is depicted in Fig. 11. It is observed that the custom and shear profiles change the peak of surface elevation by about 12% for following currents and by about −11% for opposing currents. The uniform current profile increases the peak of surface elevation in case of following current by about 4% while decreasing the peak by the same magnitude in case of opposing current.

5.3. Change in wave height and wavelength

The change in wave height and wavelength of the incident wave due to the presence of currents is investigated in this section. The investigation of the change in wave height and wavelength is carried out through two approaches.

In the first approach, change in wave height and wavelength is assessed statistically by recording the snapshots of the surface elevation within the domain (outside the relaxation zones) at a given time, and obtaining the change in wave height and wavelength by measuring their peak-to-peak variation. Similar to the previous section, in this approach, the maximum and minimum peak values are ignored and an arithmetic mean of the remaining data is taken to generate a statistically sound data set.

In the second approach, change in wave height and wavelength is further assessed by recording the snapshots of the surface elevation within the domain (outside the relaxation zones) at a given time, and reconstructing it by the Fourier series as:

$$\eta(x, t_0) = \sum_{i=1}^{n} A_i cos(\omega_i t + \delta_i), \tag{12}$$

where the surface elevation, η, is presented as a function of the x−coordinate at a given time, t_0 (Bracewell, 1989; Gallagher et al.,

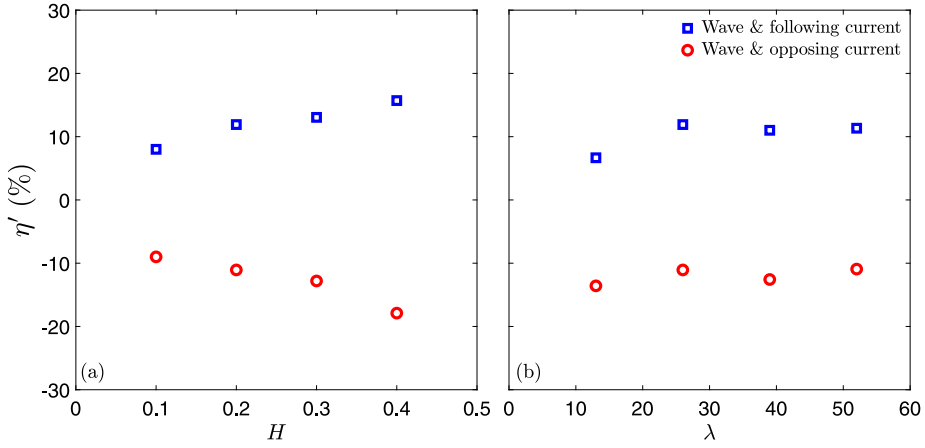

Fig. 9. Change of the peak of surface elevation, at Gauge GI, with (a) wave height and (b) wavelength, $U_f = \pm 0.14$ and $z_c = -0.5$.

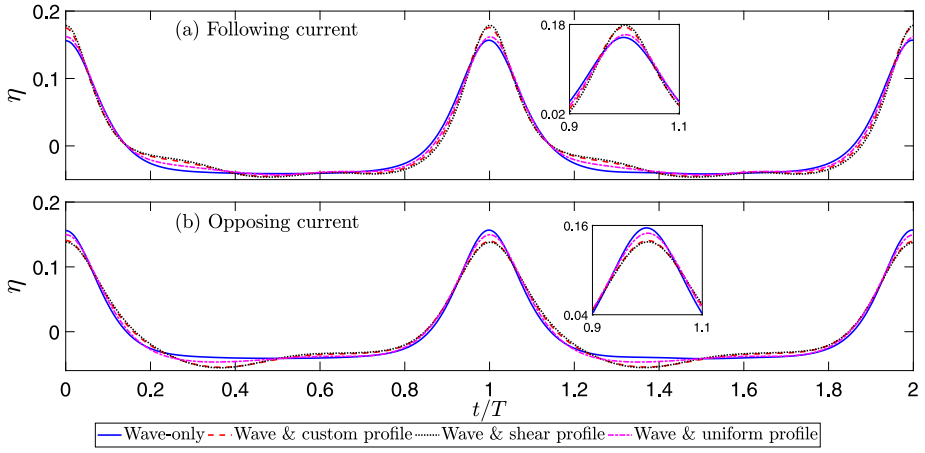

Fig. 10. Effect of different current profiles on surface elevation of wave W3, for (a) following and (b) opposing currents, recorded at Gauge GI, $H = 0.2$ and $\lambda = 26$.

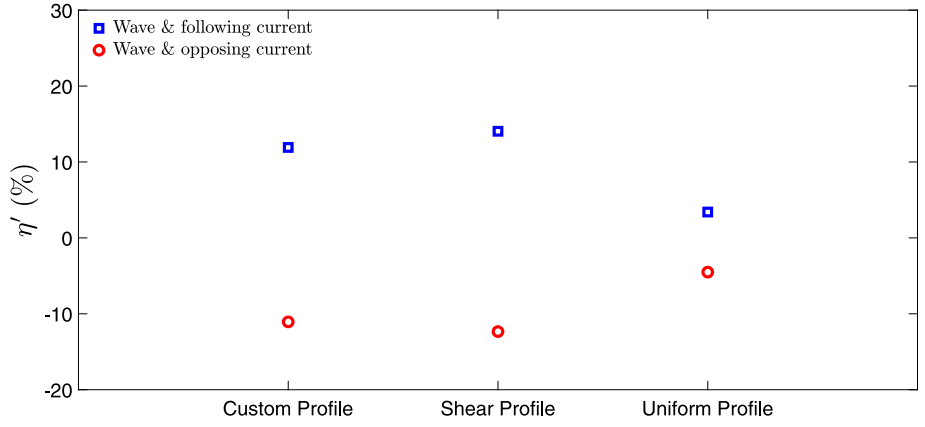

Fig. 11. Change of the peak of surface elevation of wave W3, interacting with the current configurations considered in this study, recorded at Gauge GI, $H = 0.2$ and $\lambda = 26$.

2008). Here, A_i represents the amplitudes of the first ($i = 1$) and higher ($i > 1$) harmonics, and ω_i and δ_i are the corresponding spatial frequency and phase angle, respectively. The peak frequency and amplitude are obtained from the result of the Fourier transform of the signal given in Eq. (12). A sample input signal of wave W3, and its corresponding Fourier transform output are shown in Fig. 12. In studying the change in wave height and wavelength, only the amplitudes and frequencies corresponding to the first and second harmonics ($i = 1$ and $i = 2$, respectively) are considered.

Under the first approach, the changes in wavelength and wave height are represented by $\lambda' = [(\lambda_{wc} - \lambda_w)/\lambda_w] \times 100$ and $H' = [(H_{wc} - H_w)/H_w] \times 100$, respectively, where λ_{wc} and H_{wc} are the wavelength and wave height of the wave under the influence of the current and λ_w and H_w are the wavelength and wave height of the wave in the absence of the current, i.e. these show the percentage change in wavelength and wave height when compared with wave-only cases. Under the second approach, the changes in wavelength and wave height are represented by $\lambda'_i = [(\lambda_{i(wc)} - \lambda_{i(w)})/\lambda_{i(w)}] \times 100$ and $H'_i = [(H_{i(wc)} - H_{i(w)})/H_{i(w)}] \times 100$,

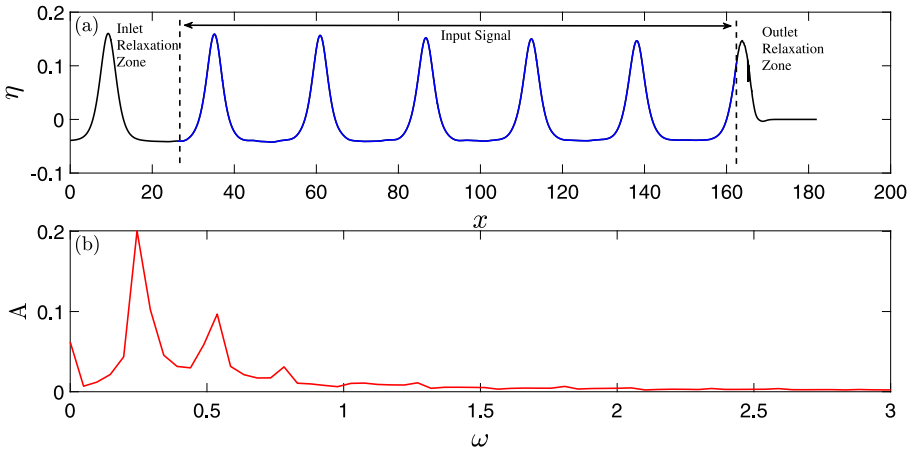

Fig. 12. Sample visual depiction of (a) snapshot of the input signal (wave W3) and (b) the Fourier transform, $H = 0.2$ and $\lambda = 26$.

respectively, where $\lambda_{i(wc)}$ and $H_{i(wc)}$ are the wavelength and wave height of the ith harmonics of the wave under the influence of the current and $\lambda_{i(w)}$ and $H_{i(w)}$ are the wavelength and wave height of the ith harmonics of the wave in the absence of the current.

5.3.1. Effect of the wave conditions

The interaction of all waves with the custom current is investigated in this subsection. Snapshots of the surface elevation within the domain as waves interact with the custom current are shown in Fig. 13. It is seen that for all wave cases considered here, a following current increases the wave height and wavelength while an opposing current reduces the same. This behaviour of change of wave height with following current is contrary to that observed in the literature for deep and intermediate water depths, see e.g., Swan et al. (2001) and Umeyama (2005, 2011). This is partially due to the relative current velocity and horizontal particle velocity under the shallow water waves considered in this study. The current velocities considered here result in a net positive effect on the horizontal particle velocity at all times of the wave cycle, unlike that in deep waters. This can be observed in Fig. 14, where the distribution of the analytical horizontal particle velocity under the wave crest and wave trough for waves W1–W7 is presented along with the following custom current velocity.

The results of the statistical assessment of peak-to-peak variation of wave height is portrayed in terms of H' in Fig. 15. It is observed in Fig. 15(a) that a following current nonlinearly increases H' from 12% to 18% as the incident wave becomes larger. An opposing current, however, changes H' from about −5% to −10% approximately, as it interacts with larger waves. It is observed that the effect of current on the wave height is more significant for larger waves. Similarly, in Fig. 15(b), it is seen that the effect of current on the wave height is more significant for longer waves. A following current increases H' from around 6% to 12% as the wavelength is doubled once, but then increases marginally when the wavelength is doubled again. An opposing current decreases H' initially and then increases it for longer waves. In all waves considered, a following current increases H', while an opposing current decreases H'.

The changes in wave height of the first and second harmonics, H_1' and H_2', for waves with various wave heights and wavelengths are shown in Fig. 16. From Fig. 16(a), it is observed that H_1' increases for larger waves, irrespective of current direction. In Fig. 16(c), it is observed that H_2' initially increases and then decreases with increasing wave height, for following and opposing current interactions.

From Fig. 16(b), it is observed that for longer waves, H_1' increases initially and then decreases, irrespective of the current direction. Fig. 16(d) shows that H_2' alternates between decreasing and increasing trends as the wave gets longer, in case of following current. H_2' registers an increment initially and then decreases for longer waves, in case of opposing current.

It is inferred that the increase in H_1' and H_2' is limited by the wave height and wavelength of the wave interacting with the current. H_1' and H_2' vary between −27% and 51% for the waves considered in this study. From Fig. 16(d), it is observed that the effect of current on the wave height of the second harmonic is smaller for longer waves. In all wave cases, H_2' obtained here is comparable in magnitude with H_1', indicating a strong influence of the current on the second harmonics of the wave, and hence, the nonlinear behaviour of the wave–current field.

The peak-to-peak variation of wavelength is analysed statistically and its results are depicted in terms of λ' in Fig. 17. It is observed that in all waves considered, a following current increases λ', while an opposing current decreases λ'. It is observed in Fig. 17(a) that a following current increases λ' by about 9% initially and then by about 11% subsequently with larger waves. In case of an opposing current, λ' changes nonlinearly from −9% to −10% for larger waves. In Fig. 17(b), it is seen that the effect of following current on λ' is largely invariant with longer waves. A following current increases λ' by about 10%, while an opposing current nonlinearly changes λ' from −10% to −9% as the wavelength increases.

The change in wavelength of the first and second harmonics, λ_1' and λ_2', with wave height and wavelength for all seven waves is presented in Fig. 18. It is observed that the change in wavelength is invariant with the height and length of the incident wave, in almost all wave conditions considered here. For the currents under consideration, an opposing current increases the wavelength of the first harmonic by 20%, while a following current has little to no effect on λ_1'. Additionally, an opposing current increases the wavelength of the second harmonic by about 10%, while a following current changes λ_2' by −10%. It is observed that λ_2' alternates between decreasing and increasing trends as the wave gets longer, as observed in case of following current for H_2' in Fig. 16(d).

5.3.2. Effect of the current profiles

The change in wave height and wavelength of wave W3 as it interacts with different current profiles, is analysed in this subsection. Based on the peak-to-peak assessment of the snapshot of surface elevation, the change in wave height, H', is reported for different current profiles in Fig. 19. It is observed that following currents have a stronger influence on H' than opposing currents. Opposing custom and shear currents change H' by about −5%, while a uniform opposing current changes H' by about −2%. The difference between H' in case of following and opposing currents is larger for custom and shear profiles when compared to uniform current profile. This indicates that the current

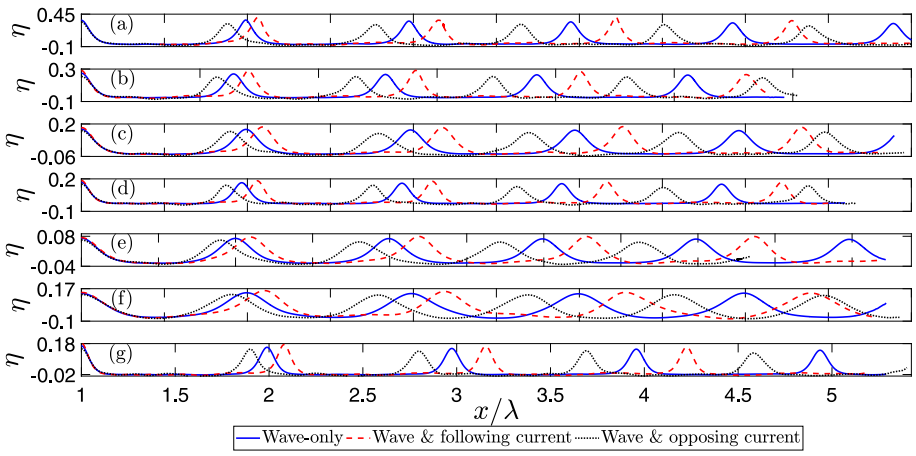

Fig. 13. Snapshots of the surface elevation (taken at time, $t = 10 \times T$) within the domain as waves (a) W1, (b) W2, (c) W3, (d) W4, (e) W5, (f) W6 and (g) W7, interact with following and opposing custom currents, $U_f = \pm 0.14$ and $z_c = -0.5$.

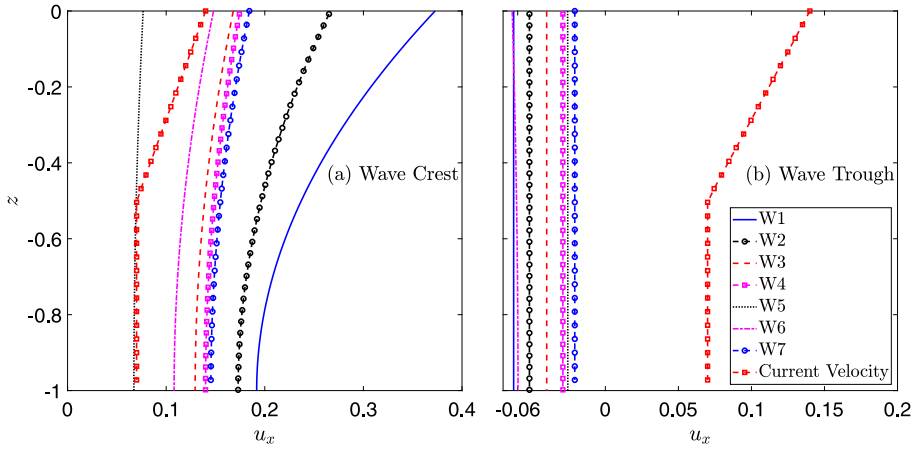

Fig. 14. Distribution of analytical horizontal particle velocity under the (a) wave crest and (b) wave trough for waves W1, W2, W3, W4, W5, W6 and W7, shown along with the following custom current velocity, $U_f = 0.14$ and $z_c = -0.5$.

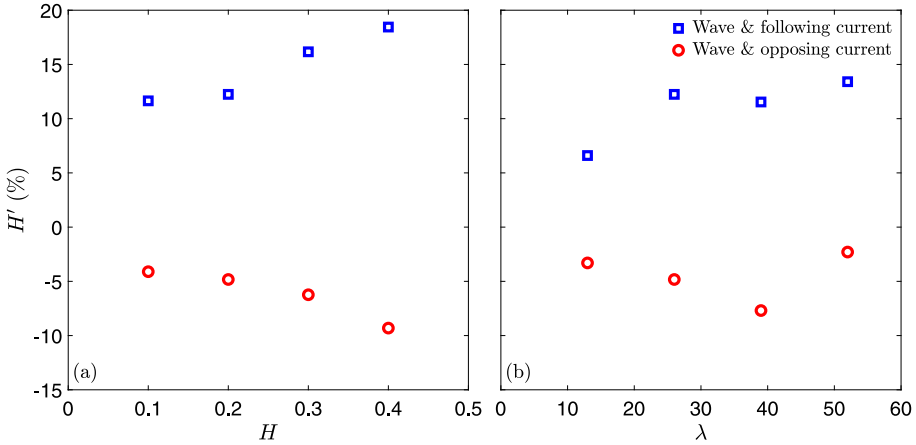

Fig. 15. Change of the wave height of the incident wave with (a) wave height and (b) wavelength, due to the presence of custom-profile current, $U_f = \pm 0.14$ and $z_c = -0.5$.

profile near the free surface has a stronger influence on the change in wave height than the current profile further away from it.

The change in the wave height of the first and second harmonics, for different current profiles under consideration, is presented in Fig. 20. It is observed that the current direction in case of a shear current has a strong influence on H_1' and H_2'. H_1' registers an increase irrespective of the current profile or direction. A shear current profile changes H_1' from 15% to 22% with change in current direction and H_2' from −40% to 40%, for the currents considered in this study. It is observed that the custom current's direction has no effect on H_1'. All current profiles have a more pronounced effect on the change in wave height of the second harmonic.

The change in wavelength obtained with the statistical assessment of the peak-to-peak variation of wavelength, λ', is reported for different

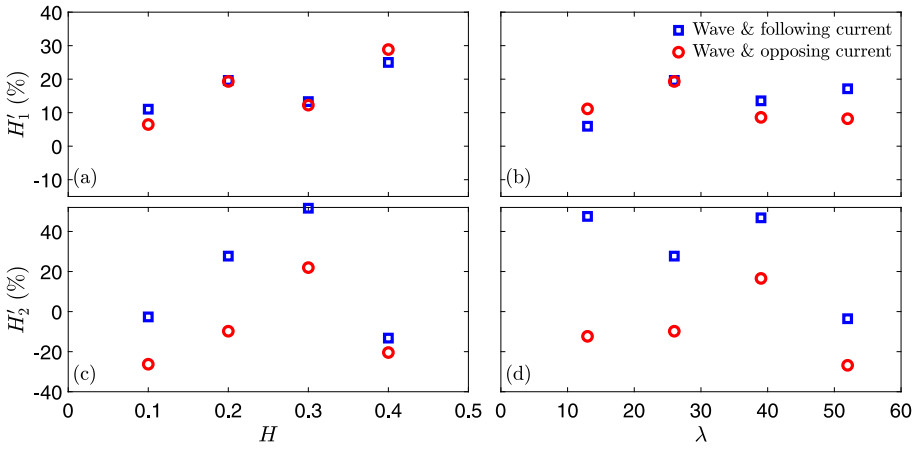

Fig. 16. Change of the wave height of the first and second harmonics with (a and c) wave height and (b and d) wavelength, due to the presence of custom-profile current, $U_f = \pm 0.14$ and $z_c = -0.5$.

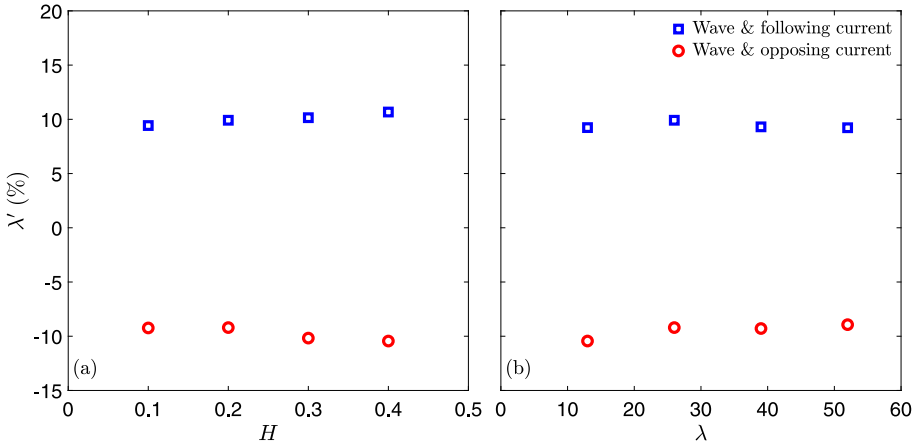

Fig. 17. Change of wavelength of the incident wave with (a) wave height and (b) wavelength, due to the presence of custom-profile current, $U_f = \pm 0.14$ and $z_c = -0.5$.

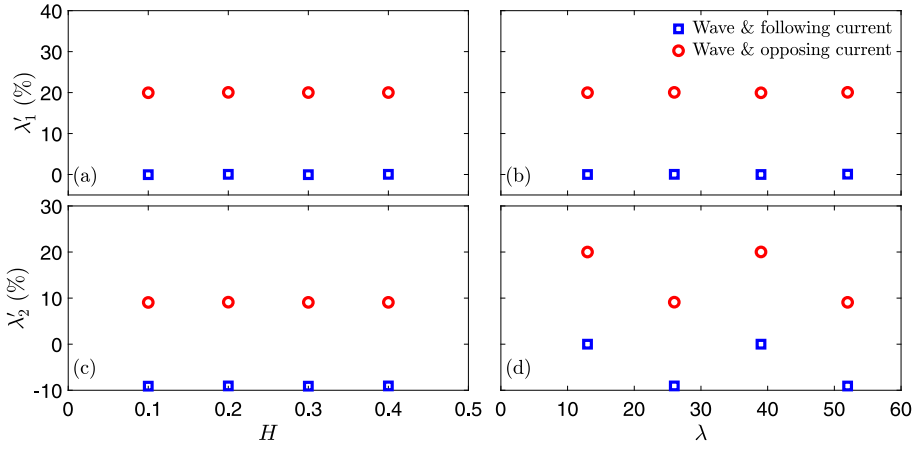

Fig. 18. Change of wavelength of the first and second harmonics with (a and c) wave height and (b and d) wavelength, due to the presence of custom-profile current, $U_f = \pm 0.14$ and $z_c = -0.5$.

current profiles in Fig. 21. It is observed that custom and shear current profiles result in very similar changes in λ', for both following and opposing current directions. For the custom current profile, λ' increases by about 10% and decreases by about 10%, in case of following and opposing currents respectively, whereas, for the shear current profile, λ' changes between ±8% approximately. In case of uniform current profile, it is observed that a following current has a stronger influence on λ' (15%) than an opposing current (−7%).

The change in wavelength of the first and second harmonics, for different current profiles under consideration, is presented in Fig. 22. It is observed that a following current does not influence λ_1', with any current profile. Opposing currents, however, increase λ_1' by 20% for all

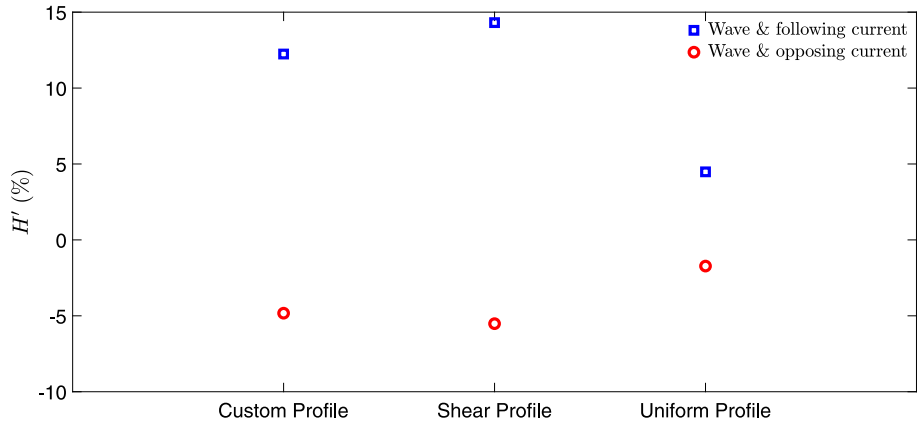

Fig. 19. Change of the wave height of the incident wave in the presence of different current profiles, $H = 0.2$ and $\lambda = 26$.

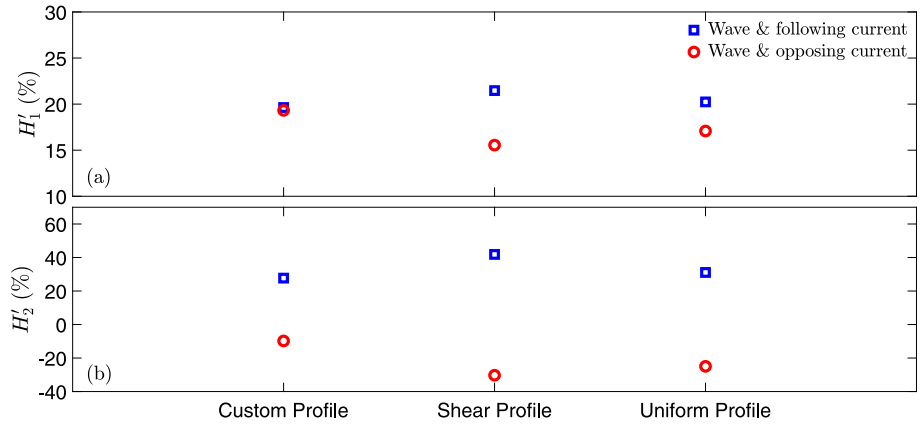

Fig. 20. Change of the wave height of the (a) first and (b) second harmonics, in the presence of different current profiles, $H = 0.2$ and $\lambda = 26$.

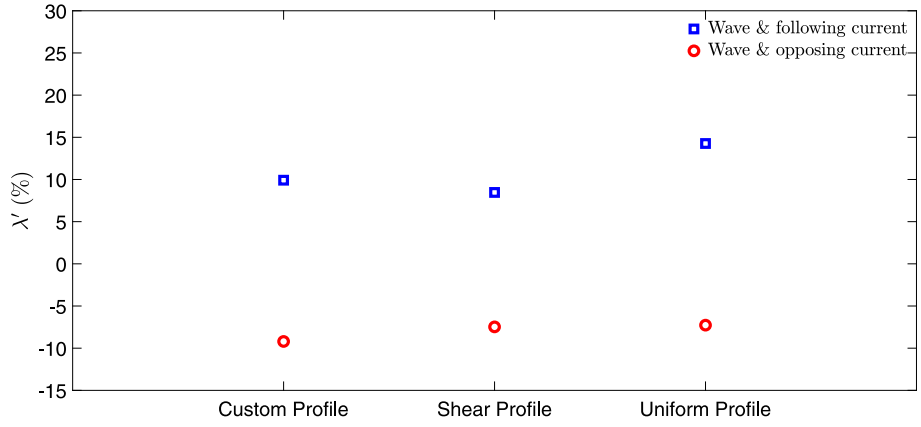

Fig. 21. Change of wavelength of the incident wave in the presence of different current profiles, $H = 0.2$ and $\lambda = 26$.

the current profiles considered here. In case of λ_2', following currents decrease the wavelength by 10% for all current profiles considered, while opposing currents increase λ_2' by 10%. This indicates that the change in wavelength of the first and second harmonics is invariant with the current profile.

5.4. Change in horizontal particle velocity

The effect of currents on horizontal particle velocity of the wave field is studied in this section. The horizontal particle velocity is recorded by the velocity sensors at depths $z = -0.33$, -0.66 and -1.0, shown in Fig. 3. The change in horizontal particle velocity is obtained using the horizontal particle velocity at $z = -0.33$, and under the peak of the wave crest, defined by $u_x' = [(u_{x(wc)} - u_{x(w)})/u_{x(w)}] \times 100$, where $u_{x(wc)}$ corresponds to the horizontal particle velocity under the influence of the current and $u_{x(w)}$ is the horizontal particle velocity in the absence of the current. u_x', therefore, is the percentage change in horizontal particle velocity when compared with the wave-only cases.

5.4.1. Effect of the wave conditions

In this subsection, the change in horizontal particle velocity of all seven waves as they interact with the custom current ($U_f = \pm 0.14$ and $z_c = -0.5$) is studied (cases W1C1, W2C1, W3C1, W4C1, W5C1, W6C1 and W7C1 in Table 4). The horizontal particle velocity of the waves,

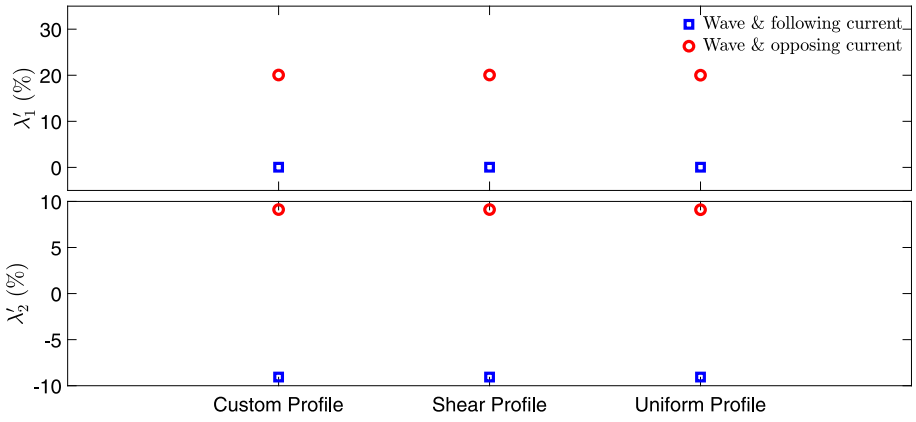

Fig. 22. Change of wavelength of the (a) first and (b) second harmonics, in the presence of different current profiles, $H = 0.2$ and $\lambda = 26$.

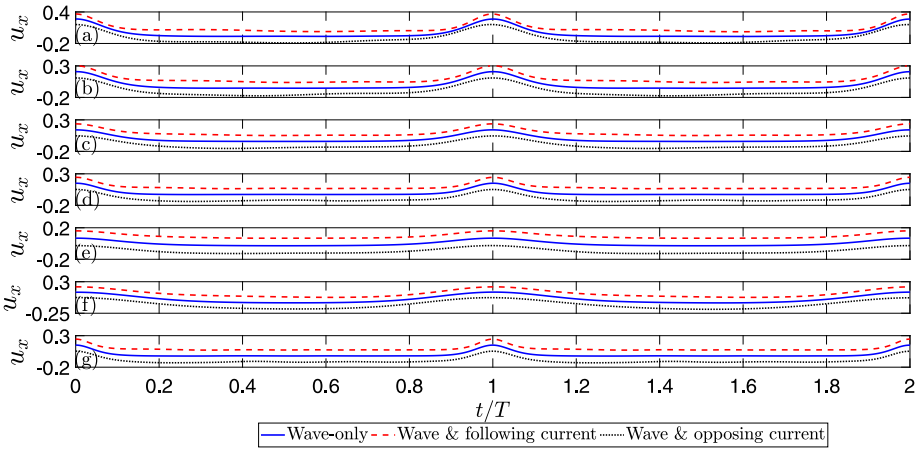

Fig. 23. Time series of horizontal particle velocity at $z = -0.33$, presented for waves (a) W1, (b) W2, (c) W3, (d) W4, (e) W5, (f) W6 and (g) W7 as they interact with following and opposing custom currents. $U_f = \pm 0.14$ and $z_c = -0.5$.

at depth $z = -0.33$, in the presence of the custom current is shown in Fig. 23. It is observed that in all cases, a following current increases the horizontal particle velocity while an opposing current decreases the horizontal particle velocity and this is expected.

The results for the change of horizontal particle velocity are shown in Fig. 24. It is observed that the effect of the current on the horizontal particle velocity becomes less remarkable for larger and longer waves. For the waves considered in this study, as the wave height is increased, u_x' changes from about 150% to 50%, in case of following current, and from −150% to −50%, in case of opposing current. This is because the change in wave height increases the horizontal particle velocity considerably. For instance, $u_{x(w)}$ at the free surface goes from 0.08 to 0.17 as H is doubled once, and then increases to 0.37 as H is doubled again. The current velocity, however, remains the same. When the wavelength is increased gradually, u_x' changes from about 80% to 50%, in case of following current, and from −80% to −50%, in case of opposing current. In this case, horizontal particle velocity, $u_{x(w)}$, at the free surface registers smaller change, going from 0.15 to 0.17 as λ is doubled once, and then increasing to 0.18 as λ is doubled again.

5.4.2. Effect of the current profiles

The change in horizontal particle velocity when wave W3 interacts with different current configurations, recorded at three different water depths is presented in Fig. 25. In Fig. 25(a), it is observed that under the uniform current profile, the horizontal particle velocity near the free surface is smaller than that of a shear or custom current profile. The difference between uniform profile and other current profiles reduces when a deeper point ($z = -0.66$ in Fig. 25(b) and $z = -1$ in Fig. 25(c)) is considered. This is because the current speed near the free surface in case of uniform current ($U_f = 0.07$) is less than the current speed near the free surface in case of custom or shear current ($U_f = 0.14$).

The change in horizontal particle velocity under the influence of different current profiles is shown in Fig. 26. It is observed that all current profiles exhibit weaker change in horizontal particle velocity at points further away from the free surface. Near the free surface (Fig. 26(a)), custom and shear current profiles elicit very similar response from u_x'. However, in case of uniform current profile, u_x' near the free surface is smaller than that observed with custom and shear profiles. As mentioned above, this results from a lower current speed near the free surface in case of uniform current. Additionally, u_x' in case of all current profiles changes nearly symmetrically for following and opposing current directions in Fig. 26. In Fig. 26(c), it is observed that at the tank floor ($z = -1$), all current profiles have little to no effect on the horizontal particle velocity, indicating that the current profile near the free surface bears greater significance than that close to the tank floor.

5.5. Change in velocity profile

The effect of currents on velocity profile of the wave field is studied in this section. The velocity profile is recorded under the wave crest and wave trough along the water depth (from SWL to the tank floor). The distribution of the vertical particle velocity under the wave crest and the wave trough for wave W3, as it interacts with following and opposing custom currents is shown in Fig. 27. It is observed in this figure that the magnitude of the vertical particle velocity distribution

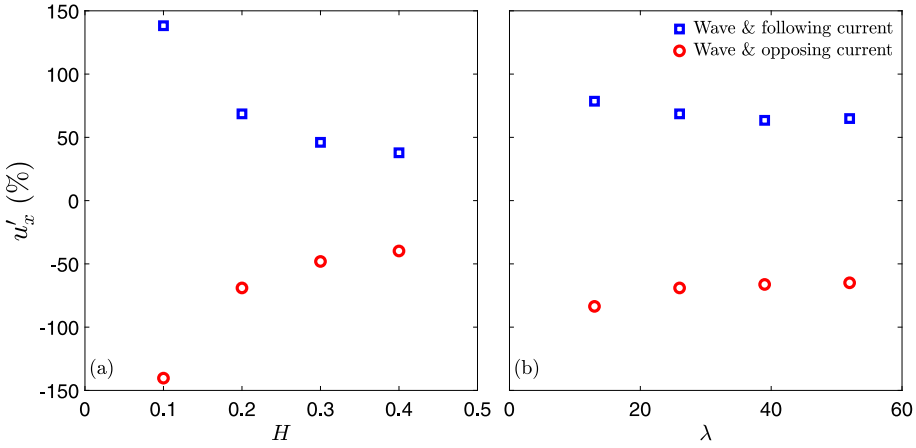

Fig. 24. Change of horizontal particle velocity recorded at $z = -0.33$, with (a) wave height and (b) wavelength, due to the presence of custom-profile current, $U_f = \pm 0.14$ and $z_c = -0.5$.

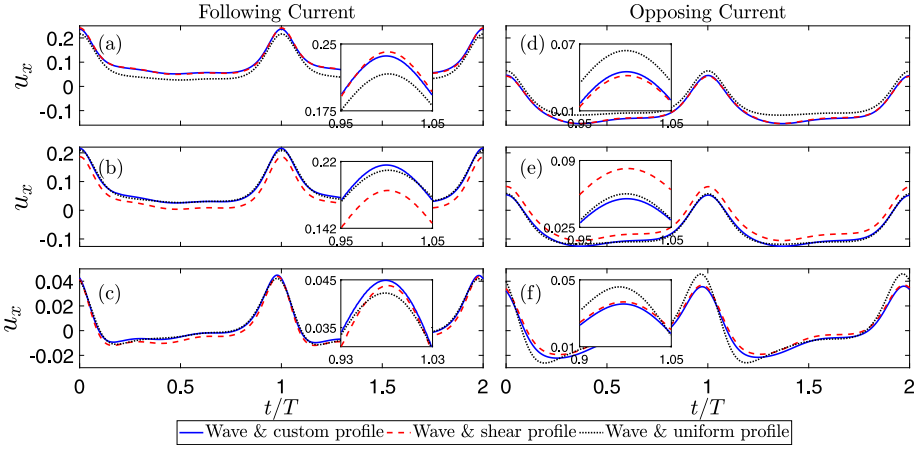

Fig. 25. Effect of different current profiles on the horizontal particle velocity recorded at (a, d) $z = -0.33$, (b, e) $z = -0.66$ and (c, f) $z = -1$, when wave W3 interacts with (a–c) following and (d–f) opposing currents, $H = 0.2$ and $\lambda = 26$.

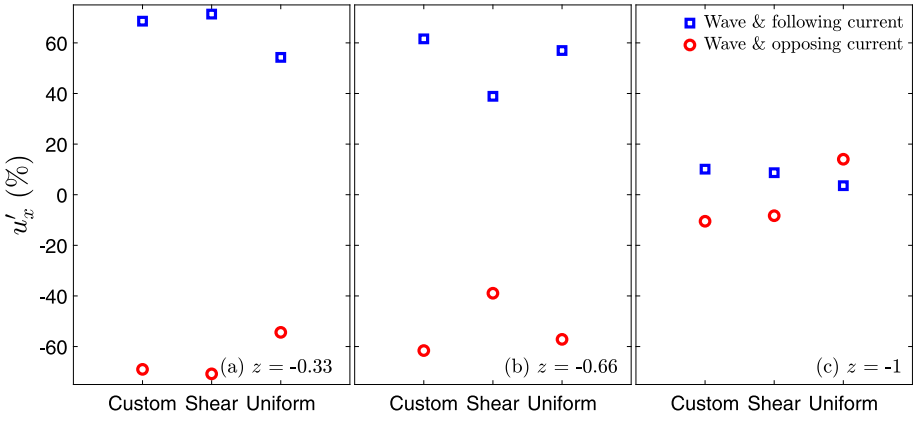

Fig. 26. Change of horizontal particle velocity recorded at (a) $z = -0.33$, (b) $z = -0.66$ and (c) $z = -1$, in the presence of different current profiles, $H = 0.2$ and $\lambda = 26$.

due to the presence of the current is relatively small when compared to the magnitude of the current velocity considered in this case.

5.5.1. *Effect of the wave conditions*

The distribution of horizontal particle velocity under the wave crest and the wave trough, for all seven waves, as they interact with following and opposing custom current profiles, is shown in Fig. 28. It is observed that under the wave crest and the wave trough, the distribution of the horizontal particle velocity closely follows the current profile. Further, the percentage change in horizontal particle velocity, u'_x, is presented with the water depth for wave W5 (Fig. 28(e, l)). It is observed that the under the wave trough, the distribution of u'_x registers a larger change (up to 8 times difference) when compared to its distribution under the wave crest (up to 2 times difference). This

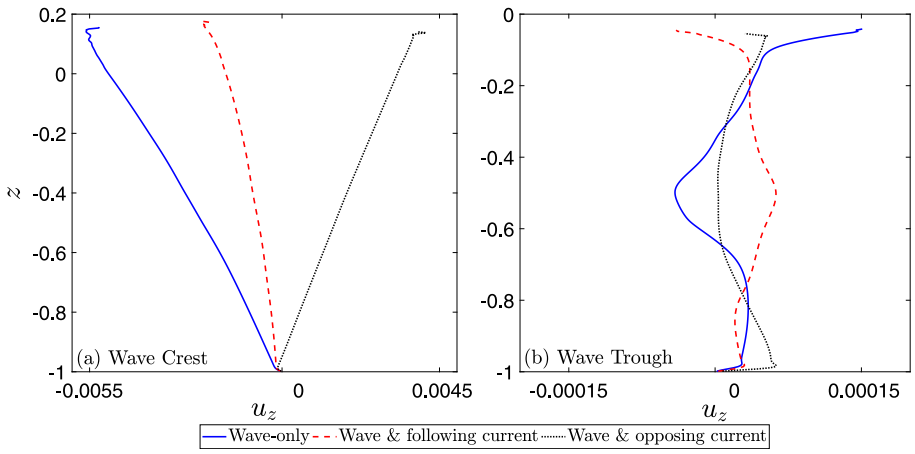

Fig. 27. Distribution of the vertical particle velocity (u_z) under the (a) wave crest and (b) wave trough for wave W3, as it interacts with following and opposing custom currents, $U_f = \pm 0.14$ and $z_c = -0.5$.

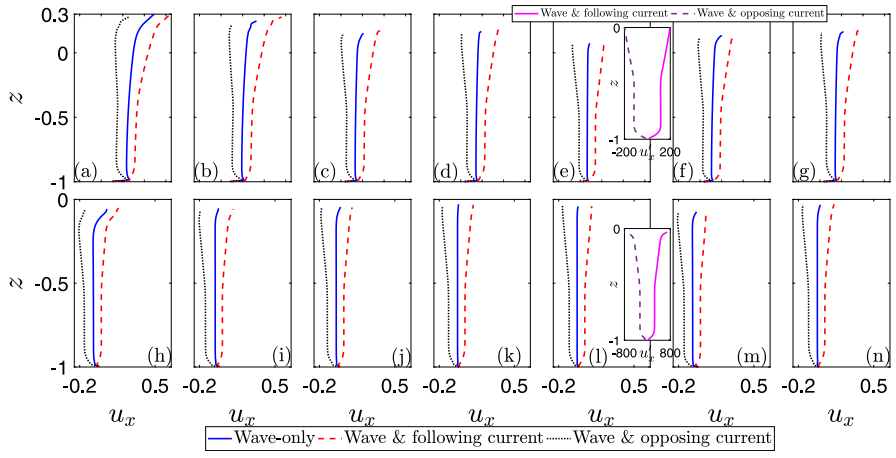

Fig. 28. Distribution of the horizontal particle velocity under the (a–g) wave crest and (h–n) wave trough, for waves (a, h) W1, (b, i) W2, (c, j) W3, (d, k) W4, (e, l), W5, (f, m) W6 and (g, n) W7, as they interact with following and opposing custom currents, $U_f = \pm 0.14$ and $z_c = -0.5$.

is expected because in the absence of current, the horizontal particle velocity under the wave trough is smaller than that under the wave crest. It is also observed that wave cases that have the same wave height (W3, W4, W6 and W7) depict very similar velocity profiles.

The distribution of vertical particle velocity under the wave crest and the wave trough, for all seven wave cases, as they interact with following and opposing custom current profiles, is shown in Fig. 29. It is observed that the magnitude of vertical particle velocity remains quite small compared to the magnitude of the current velocity and no conclusive trend is seen in its behaviour.

5.5.2. Effect of the current profiles

The distribution of the horizontal particle velocity under the wave crest and wave trough, as wave W3 interacts with custom, shear and uniform current profiles, is presented in Fig. 30. Here, it is observed that the influence of a all current profiles results in a symmetrical distribution of the following and opposing velocity profiles about the wave-only case. Further, the results of linear superposition of horizontal particle velocity due to the wave, u_w (Eq. (6)), and the horizontal particle velocity due to the current, u_c, are also included in Fig. 30. It is inferred that the distribution of horizontal particle velocity obtained from the wave–current field using the NS solver differs from that obtained by linear superposition of wave and current velocities. However, it appears that the linear superposition of the undisturbed wave and current horizontal particle velocity is in fact in close agreement with the wave–current field observations for the following currents (particularly under the wave trough).

5.6. Change in pressure

The effect of currents on the pressure field is studied in this section. The pressure is recorded by numerical pressure sensors at depths $z = -0.33$, -0.66 and -1.0, shown in Fig. 3. In order to obtain the hydrodynamic pressure, P, the hydrostatic pressure at the respective depths (from the SWL) is subtracted from the total pressure, i.e. $P = p + \rho g z$, where z is the vertical coordinate of the point selected for analysis. The change in pressure is obtained using the hydrodynamic pressure at the peak of the wave crest and is given by $P' = [(P_{wc} - P_w)/P_w] \times 100$, where P_{wc} is the hydrodynamic pressure under the influence of the current and P_w is the hydrodynamic pressure in the absence of the current. P', therefore, is the percentage change in hydrodynamic pressure when compared with wave-only cases.

5.6.1. Effect of the wave conditions

In this subsection, the change of hydrodynamic pressure of all seven waves as they interact with the custom current is studied i.e. the interaction of the waves with the current with $U_f = \pm 0.14$ and $z_c = -0.5$ (cases W1C1, W2C1, W3C1, W4C1, W5C1, W6C1 and W7C1 in Table 4). The hydrodynamic pressure of the waves at depth $z = -0.33$ in the presence of the current is shown in Fig. 31. An enlarged view of the wave crest is also presented for all seven wave cases. It is observed that a following current increases the hydrodynamic pressure while an opposing current decreases the hydrodynamic pressure, in all wave cases under consideration.

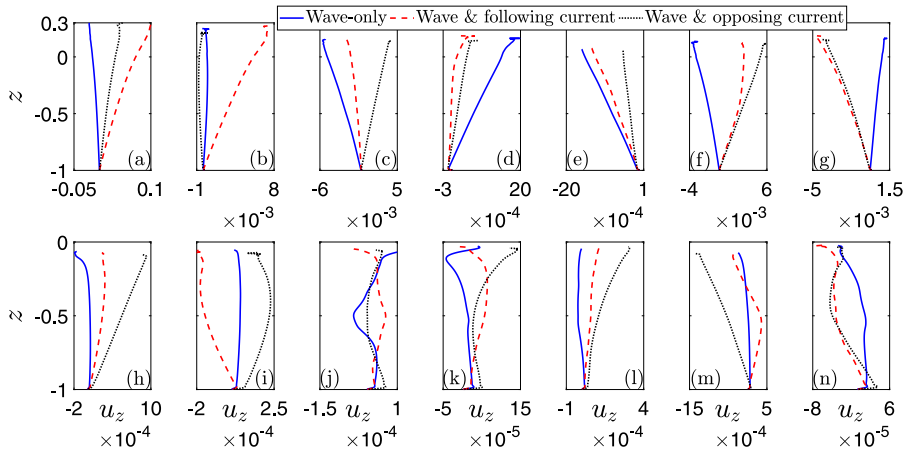

Fig. 29. Distribution of the vertical particle velocity under the (a–g) wave crest and (h–n) wave trough, for waves (a, h) W1, (b, i) W2, (c, j) W3, (d, k) W4, (e, l), W5, (f, m) W6 and (g, n) W7, as they interact with following and opposing custom currents, $U_f = \pm 0.14$ and $z_c = -0.5$.

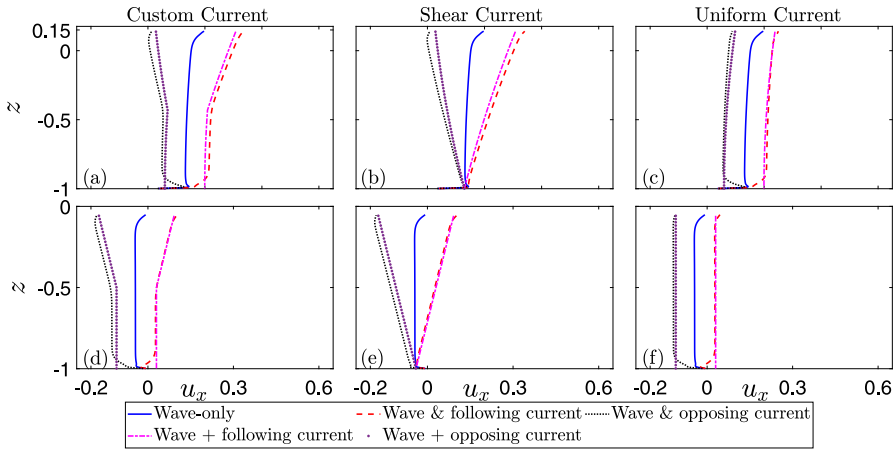

Fig. 30. Distribution of the horizontal particle velocity under the (a–c) wave crest and (d–f) wave trough, as wave W3 interacts with (a, d) custom, (b, e) shear and (c, f) uniform current profiles, $H = 0.2$ and $\lambda = 26$.

The effect of custom current on the change in hydrodynamic pressure recorded at $z = -0.33$, for all seven waves, as they interact with following and opposing currents, is shown in Fig. 32. Here, variation of P' with wave height and wavelength is presented. It is observed that in case of following current, the hydrodynamic pressure increases initially as the wave height is doubled and then reduces marginally when the wave height is doubled again. In case of an opposing current, P' changes from −10% to −15% as the wave height is increased gradually. Fig. 32(b) shows that in case of following current, P' increases initially with larger λ. However, it appears that for longer waves ($\lambda > 26$ here), P' is invariant with λ. For opposing currents, P' increases with λ initially, and then reduces marginally for $\lambda > 26$.

5.6.2. Effect of the current profiles

The effect of different current profiles on the hydrodynamic pressure recorded at three different water depths is shown in Fig. 33. It is observed that under the influence of a following current, the hydrodynamic pressure is smaller in case of uniform current profile when compared with a shear or custom current profile. Whereas, under the influence of an opposing current, the hydrodynamic pressure is larger in case of uniform current when compared with a shear or custom current profile. This indicates that the current direction modifies the pressure field significantly.

The change in hydrodynamic pressure under the influence of different current profiles is shown in Fig. 34. All current profiles exhibit similar change in P' at points further away from the free surface. It is inferred that the change in hydrodynamic pressure due to currents is invariant with water depth. Custom and shear current profiles result in very similar changes to P'. It is observed that in case of following current, the custom and shear current profiles change the hydrodynamic pressure by about 11% and 13%, respectively. In case of opposing current, the custom and shear current profiles change the hydrodynamic pressure by about −11% and −13%, respectively. Uniform opposing current has the weakest influence on the hydrodynamic pressure at all points of observation.

6. Conclusions

A numerical wave–current tank is created to assess the effect of current profile and current direction on the shallow water wave fields. Different parameters pertaining to the wave field including surface elevation, wavelength, wave height, horizontal particle velocity, velocity profile and pressure are investigated. The effect of the incident wave height and wavelength on wave–current interactions is also assessed. Seven waves and six current configurations are considered in the study. The shallow water waves are generated using the Cnoidal wave theory and the wave–current maker is developed using the principle of linear superposition. Based on the results obtained, it is observed that the wave field undergoes significant changes upon encountering a following or opposing current.

The change of surface elevation as the wave interacts with currents is studied and it is observed that an opposing current reduces the peak

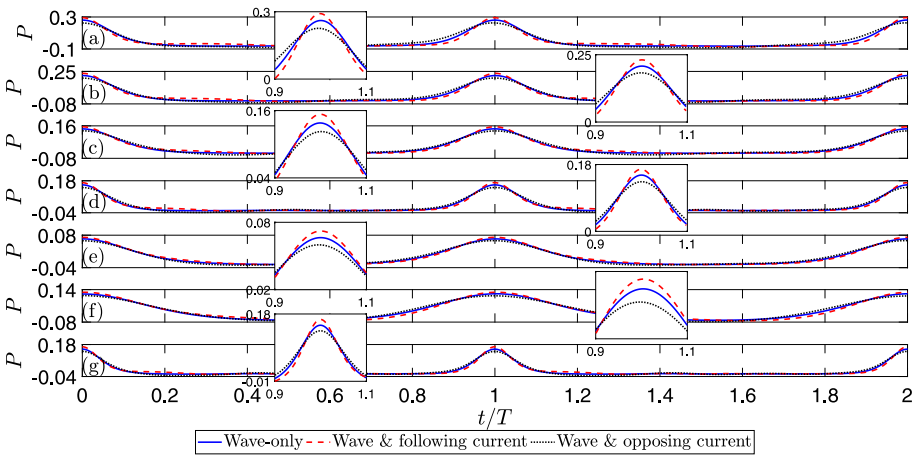

Fig. 31. Time series of hydrodynamic pressure at $z = -0.33$, for waves (a) W1, (b) W2, (c) W3, (d) W4, (e) W5, (f) W6 and (g) W7, as they interact with following and opposing custom currents, $U_f = \pm 0.14$ and $z_c = -0.5$.

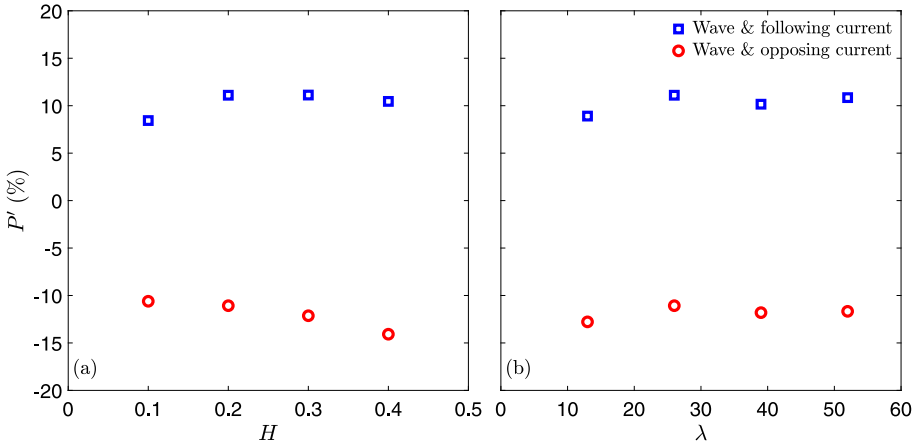

Fig. 32. Change of hydrodynamic pressure recorded at $z = -0.33$, with (a) wave height and (b) wavelength, due to the presence of custom-profile current, $U_f = \pm 0.14$ and $z_c = -0.5$.

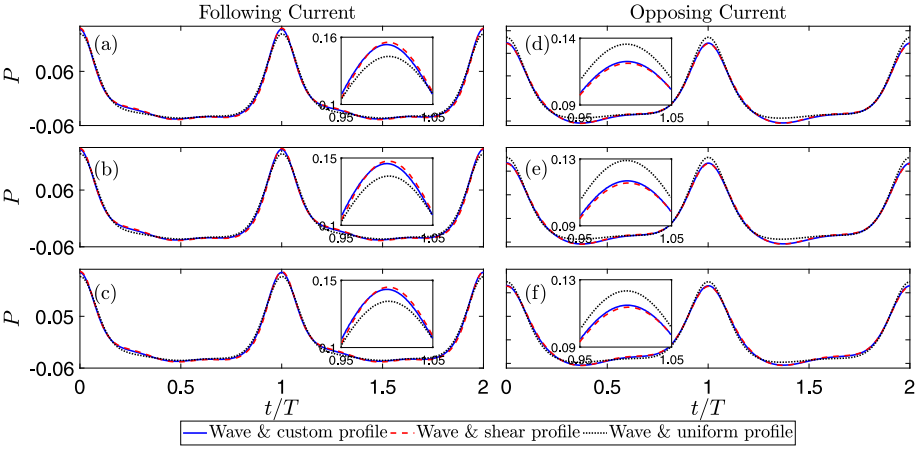

Fig. 33. Effect of different current profiles on the hydrodynamic pressure recorded at (a, d) $z = -0.33$, (b, e) $z = -0.66$ and (c, f) $z = -1$, when wave W3 interacts with (a–c) following and (d–f) opposing currents, $H = 0.2$ and $\lambda = 26$.

of the surface elevation whereas a following current enlarges the peak. It is also inferred that currents interacting with larger waves have a more pronounced effect on the change of surface elevation. Following currents interacting with longer waves have a significant impact on the change of surface elevation initially, and then are invariant with wavelength for $\lambda > 26$. The effect of opposing currents on the change of surface elevation is largely invariant with wavelength. Custom and shear current profiles result in very similar changes in surface elevation indicating that the current profile near the free surface has the dominant effect on the wave field.

For the currents selected in this study, it is seen that following currents increase the wave height and wavelength, while opposing

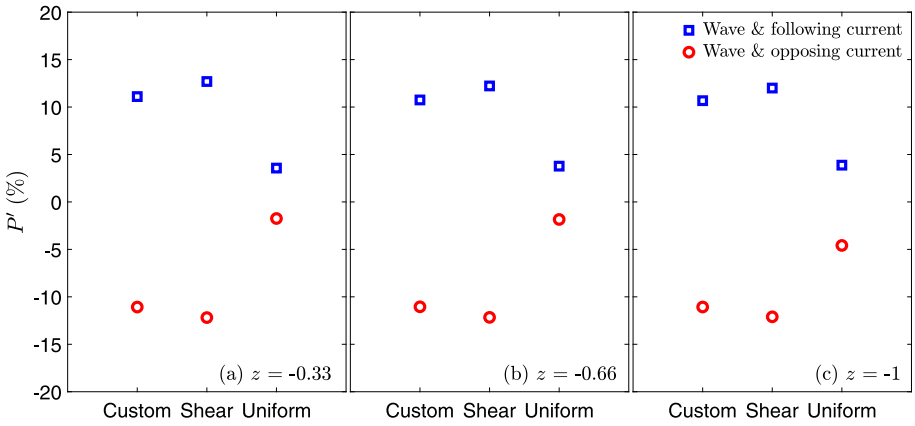

Fig. 34. Change of hydrodynamic pressure recorded at (a) $z = -0.33$, (b) $z = -0.66$ and (c) $z = -1$, in the presence of different current profiles, $H = 0.2$ and $\lambda = 26$.

currents decrease the wave height and wavelength. The change of wave height is observed to be opposite to that seen in the literature for deep water waves, and this is due to the current velocity resulting in a net positive horizontal particle velocity at all times. This indicates that the effect of current on the change of wave field varies significantly depending on the wave–current conditions. Based on the results obtained for the current velocities and profiles chosen here, it is observed that when most waves interact with following and opposing currents, the change in wave height of the first and second harmonics increases initially and then decreases with increasing wave height and wavelength. Custom and shear current profiles strongly influence H' indicating that the current profile near the free surface is more dominant. It is found that the current profile strongly influences the change in wave height of the second harmonics when waves interact with following currents. The change in wavelength of the first and second harmonics seem invariant when the incoming waves become larger and longer.

A study of the effect of currents on horizontal particle velocity shows that currents interacting with larger and longer waves have weaker effect on the change in horizontal particle velocity, u'_x. Additionally, all current profiles exhibit weaker change in horizontal particle velocity at points further away from the free surface. All current profiles considered in this study result in nearly symmetrical distribution of u'_x, when assessed near the free surface. It is concluded that the current profile near the free surface bears greater significance on u'_x than that close to the tank floor.

A study of the velocity profile under the wave crest shows that the distribution of horizontal particle velocity closely follows the current profile. The interaction between wave W3 and all three current profiles resulted in a symmetrical distribution of horizontal particle velocity profile about the wave-only case. It is inferred that a summation of wave and current velocities does not depict correctly the velocities under combined wave–current interaction.

A study of the effect of currents on hydrodynamic pressure shows that currents interacting with larger waves have a stronger effect on the change in hydrodynamic pressure. P' initially varies with increase in wavelength, but then remains invariant for $\lambda > 26$. The current direction plays a significant role in the change of the pressure field.

CRediT authorship contribution statement

Arun Kumar: Formal analysis, Investigation, Methodology, Software, Validation, Visualization, Writing – original draft, Writing – review & editing. **Masoud Hayatdavoodi:** Conceptualization, Formal analysis, Investigation, Methodology, Resources, Software, Supervision, Writing – original draft, Writing – review & editing.

Declaration of competing interest

The authors declare that they have no known competing financial interests or personal relationships that could have appeared to influence the work reported in this paper.

Data availability

The data that support the findings of this study are available within the article.

Acknowledgements

This work is partially based on funding from the Kaluosi-Qianghai New Energies Ltd. of China and Energy Technology Partnership (ETP) of Scotland. These funding are gratefully acknowledged. Any findings and opinions contained in this present paper are those of the author and do not necessarily reflect the opinions of the funding agencies.

References

Bai, J., Ma, N., Gu, X., 2017. Study of interaction between wave–current and the horizontal cylinder located near the free surface. Appl. Ocean Res. 67, 44–58.
Bracewell, R.N., 1989. The Fourier transform. Sci. Am. 260, 86–95.
Brevik, I., 1980. Flume experiment on waves and currents II. Smooth bed. Coast. Eng. 4, 89–110.
Brevik, I., Aas, B., 1979. Flume experiment on waves and currents. I. Rippled bed. Coast. Eng. 3, 149–177.
Carollo, C., Astin, I., Graff, J., 2005. Vertical structure of currents in the vicinity of the Iceland-Scotland ridge. Ann. Geophys. 23, 1963–1975.
Chen, Q., Madsen, P.A., Basco, D.R., 1999. Current effects on nonlinear interactions of shallow-water waves. J. Waterw. Port Coast. Ocean Eng. 125, 176–186.
Chen, L.F., Stagonas, D., Santo, H., Buldakov, E.V., Simons, R.R., Taylor, P.H., Zang, J., 2019. Numerical modelling of interactions of waves and sheared currents with a surface piercing vertical cylinder. Coast. Eng. 145, 65–83.
Chen, L.F., Zang, J., Hillis, A.J., Morgan, G.C.J., Plummer, A.R., 2014. Numerical investigation of wave-structure interaction using OpenFOAM. Ocean Eng. 88, 91–109.
Chen, H., Zou, Q., 2019. Effects of following and opposing vertical current shear on nonlinear wave interactions. Appl. Ocean Res. 89, 23–35.
Choi, W., 2003. Strongly nonlinear long gravity waves in uniform shear flows. Phys. Rev. E 68, 026–305.
Dalrymple, R.A., 1974. Water waves on a bilinear shear current. Coast. Eng. Proc. 1, 36.
Duan, W.Y., Wang, Z., Zhao, B.B., Ertekin, R.C., Yang, W.Q., 2018. Steady solution of solitary wave and linear shear current interaction. Appl. Math. Model. 60, 354–369.
Faraci, C., Musumeci, R.E., Marino, M., Ruggeri, A., Carlo, L., Jensen, B., Foti, E., Barbaro, G., Elsaßer, B., 2021. Wave and current dominated combined orthogonal flows over fixed rough beds. Cont. Shelf Res. 220, 104403.
Faraci, C., Scandura, P., Musumeci, R., Foti, E., 2018. Waves plus currents crossing at a right angle: near-bed velocity statistics. J. Hydraul. Res. 56, 464–481.
Fenton, J.D., 1985. A fifth-order stokes theory for steady waves. J. Waterw. Port Coast. Ocean Eng. 111, 216–234.

Ferziger, J.H., Perić, M., Street, R.L., 2002. Computational Methods for Fluid Dynamics, Vol. 3. Springer.
Fredsøe, J., Andersen, K.H., Sumer, B.M., 1999. Wave plus current over a ripple-covered bed. Coast. Eng. 38, 177–221.
Gallagher, T.A., Nemeth, A.J., Hacein-Bey, L., 2008. An introduction to the Fourier transform: relationship to MRI. Am. J. Roentgenol. 190, 1396–1405.
Grue, J., 1992. Nonlinear water waves at a submerged obstacle or bottom topography. J. Fluid Mech. 244, 455–476.
Guyenne, P., 2017. A high-order spectral method for nonlinear water waves in the presence of a linear shear current. Comput. & Fluids 154, 224–235.
Hayatdavoodi, M., Ertekin, R.C., Valentine, B.D., 2017. Solitary and cnoidal wave scattering by a submerged horizontal plate in shallow water. AIP Adv. 7, 065212.
Hayatdavoodi, M., Seiffert, B., Ertekin, R.C., 2015. Experiments and calculations of cnoidal wave loads on a flat plate in shallow-water. J. Ocean Eng. Mar. Energy 1, 77–99.
Hirt, C.W., Nichols, B.D., 1981. Volume of fluid (VOF) method for the dynamics of free boundaries. J. Comput. Phys. 39, 201–225.
Hsiao, Y., Tsai, C.L., Chen, Y.L., Wu, H.L., Hsiao, S.C., 2020. Simulation of wave–current interaction with a sinusoidal bottom using openfoam. Appl. Ocean Res. 94, 101998.
Hsu, H.C., Chen, Y.Y., Hsu, J.R.C., Tseng, W.J., 2009. Nonlinear water waves on uniform current in lagrangian coordinates. J. Nonlinear Math. Phys. 16, 47–61.
Jacobsen, N.G., Fuhrman, D.R., Fredsøe, J., 2012. A Wave Generation Toolbox for the Open-Source CFD Library: OpenFOAM. Internat. J. Numer. Methods Fluids 70, 1073–1088.
Jeans, G., Grant, C., Feld, G., 2003. Improved current profile criteria for deep-water riser design. J. Offshore Mech. Arct. Eng. 125, 221–224.
Jeans, G., Prevosto, M., Harrington-Missin, L., Maisondieu, C., Herry, C., Lima, J.A.M., 2012. Deep-water current profile data sources for riser engineering offshore Brazil. In: International Conference on Offshore Mechanics and Arctic Engineering. Rio de Janeiro, Brazil, pp. 155–168.
Kemp, P.H., Simons, R.R., 1982. The interaction between waves and a turbulent current: waves propagating with the current. J. Fluid Mech. 116, 227–250.
Kumar, A., Hayatdavoodi, M., 2023. On wave–current interaction in deep and finite water depths. J. Ocean Eng. Mar. Energy To appear.
Liau, J.M., Roland, A., Hsu, T.W., Ou, S.H., Li, Y.T., 2011. Wave refraction-diffraction effect in the wind wave model WWM. Coast. Eng. 58, 429–443.
Lim, K.Y., Madsen, O.S., 2016. An experimental study on near-orthogonal wave–current interaction over smooth and uniform fixed roughness beds. Coast. Eng. 116, 258–274.
Lodahl, C.R., Sumer, B.M., Fredsøe, J., 1998. Turbulent combined oscillatory flow and current in a pipe. J. Fluid Mech. 373, 313–348.
Markus, D., Wüchner, R., Bletzinger, K.U., 2013. A numerical investigation of combined wave–current loads on tidal stream generators. Ocean Eng. 72, 416–428.
Petrotta, C., Faraci, C., Scandura, P., Foti, E., 2018. Experimental investigation on sea ripple evolution over sloping beaches. Ocean Dyn. 68, 1221–1237.
Ruggeri, A., Faraci, C., 2022. Collinear interaction of waves and current in the presence of ripple in the U-tube. Water 14, 470.
Sheikh, R., Brown, A., 2010. Extreme vertical deepwater current profiles in the south China sea, offshore Borneo. In: International Conference on Offshore Mechanics and Arctic Engineering. Shanghai, China, pp. 585–595.
Shen, C.Y., Evans, T.E., Mied, R.P., Chubb, S.R., 2008. A velocity projection framework for inferring shallow water currents from surface tracer fields. Cont. Shelf Res. 28, 849–864.
Son, S., Lynett, P.J., 2014. Interaction of dispersive water waves with weakly sheared currents of arbitrary profile. Coast. Eng. 90, 64–84.
Soulsby, R.L., Hamm, L., Klopman, G., Myrhaug, D., Simons, R.R., Thomas, G.P., 1993. Wave–current interaction within and outside the bottom boundary layer. Coast. Eng. 21, 41–69.
Svendsen, I.A., Jonsson, I.G., 1976. Hydrodynamics of Coastal Regions. Den Private Ingeniørfond, Technical University of Denmark.
Swan, C., 1990. An experimental study of wave on a strongly sheared current profile. Coast. Eng. Proc. 1.
Swan, C., Cummins, I.P., James, R.L., 2001. An experimental study of two-dimensional surface water waves propagating on depth-varying currents. Part 1. Regular waves. J. Fluid Mech. 428, 273–304.
Tao, J., Han, G., 2002. Effects of water wave motion on pollutant transport in shallow coastal water. Sci. China Ser. E 45, 593–605.
Thomas, G., 1981. Wave–current interactions: an experimental and numerical study. Part 1. Linear waves. J. Fluid Mech. 110, 457–474.
Thomas, G., 1990. Wave–current interactions: an experimental and numerical study. Part 2. Nonlinear waves. J. Fluid Mech. 216, 505–536.
Toffoli, A., Waseda, T.H.T.K.D., Houtani, H., Kinoshita, T., Collins, K., Proment, D., Onorato, M., 2013. Excitation of rogue waves in a variable medium: An experimental study on the interaction of water waves and currents. Phys. Rev. E 87, 051201.
Umeyama, M., 2005. Reynolds stresses and velocity distributions in a wave–current coexisting environment. J. Waterw. Port Coast. Ocean Eng. 131, 203–212.
Umeyama, M., 2009. Changes in turbulent flow structure under combined wave–current motions. J. Waterw. Port Coast. Ocean Eng. 135, 213–227.
Umeyama, M., 2011. Coupled PIV and PTV measurements of particle velocities and trajectories for surface waves following a steady current. J. Waterw. Port Coast. Ocean Eng. 137, 85–94.
Wang, Z., Zhao, B.B., Duan, W.Y., Ertekin, R.C., Hayatdavoodi, M., Zhang, T.Y., 2020. On solitary wave in nonuniform shear currents. J. Hydrodyn. 32, 800–805.
Yoon, S.B., Liu, P.L.F., 1989. Interactions of currents and weakly nonlinear water waves in shallow water. J. Fluid Mech. 205, 397–419.
Zhang, J., Zhang, Y., Jeng, D.S., Liu, P.L.F., Zhang, C., 2014. Numerical simulation of wave–current interaction using a RANS solver. Ocean Eng. 75, 157–164.
Zhang, J., Zheng, J., Jeng, D.S., Guo, Y., 2015. Numerical simulation of solitary wave propagation over a steady current. J. Waterw. Port Coast. Ocean Eng. 141, 04014041.